MOLECULAR ORDER AT POLYMER SURFACES

VIA

X-RAY PHOTOELECTRON SPECTROSCOPY

by

Leonardo C. Lopez Barragan

thesis submitted to the Faculty of the
Virginia Polytechnic Institute and State University
in partial fulfillment of the requirements for the degree of
MASTER OF SCIENCE
in
Materials Engineering

APPROVED:

David W. Dwight, Chairman

Garth L. Wilkes

James P. Wightman

Jack L. Lytton

October, 1984
Blacksburg, Virginia

MOLECULAR ORDER AT POLYMER SURFACES

VIA

X-RAY PHOTOELECTRON SPECTROSCOPY

by

Leonardo C. Lopez Barragan

(ABSTRACT)

Molecular order in surfaces is probed for several different repeat unit chemistries. X-ray Photoelectron Spectroscopy (XPS) is used, particularly with angular dependence, to obtain the compositional gradient information from the top 6 nm of the surface. It is found that all materials investigated present some kind of preferential and reproducible ordering effect. The ordering effect can be present in different forms, such as preferential segregation of a crystalline block to the surface, segregation of a component of different crystalline structure to the surface or orientation of a backbone segment of the polymer towards the surface of the specimen. Polyethylene terephthalate shows an increasing amount of crystalline cyclic oligomer at the surface as the degree of crystallinity of the matrix increases. Block copolyesters containing saturated and unsaturated blocks present the saturated blocks

preferentially segregated toward the surface. Crystalline ethylene/chlorotrifluoroethylene alternating copolymer shows the preferential orientation of ethylene groups closer to the surface. The linear polyurethanes studied reveal the surfaces enriched with soft segments, whereas no enrichment was observed for a crosslinked polyurethane.

Lovingly dedicated to my wife inexhaustible source of strength and inspiration to me.

ACKNOWLEDGEMENTS

I wish to express my sincere appreciation and deep gratitude to Prof. D. W. Dwight for his understanding, support and suggestions throughout the course of this thesis and my graduate studies at Tech. I also wish to extend my gratitude to Prof. J. P. Wightman, Prof. G. L. Wilkes and Prof. J. L. Lytton for their critical comments and helpful suggestions on this work.

My gratitude goes to Dr. Chi Tran and Prof. G. L. Wilkes for their generosity in providing me with some of the polymer samples used in this investigation. Special thanks are also due to Prof. M. B. Polk of the Department of Chemistry at Atlanta University, for sharing the polyester samples that were used in this thesis. I would like to convey my great appreciation to for sharing his knowledge of the XPS instrument, backbone of the whole investigation.

Deep appreciation goes to all my colleagues and friends at the Nanoprobe Laboratory for making graduate school a wonderful experience.

Finally, my heartfelt thanks go to my parents,
and and my wife's parents,
and for their ever present love and support.

TABLE OF CONTENTS

LIST OF FIGURES

Figure

page

LIST OF TABLES

Chapter I

INTRODUCTION

A solid, by definition, is a portion of matter that is rigid and resists stress. The solid is in contact with its surroundings by means of its surface. Although surface has several meanings, of which only the geometrical definition is precise, in the forthcoming piece of work the word "surface" is going to denote the outermost few tens of angstroms of the solid. This is an important concept since it has been shown that the surface of a solid is not always representative of the composition or morphology of the bulk of the solid.

The surface properties of a solid are quite important in a great number of applications, namely adhesion science[1], friction and wear[2], printing[3], corrosion[4], textiles[5], catalysis, bio-implants, etc. For example, materials for biomedical applications must have appropriate surface properties (blood compatibility) in addition to adequate bulk properties, since the surface of the implant is in contact with the organism. It has been indicated that the physico-chemical surface structure of the polymeric implant is responsible for many of the implant failures[6-8]. In adhesion science, the surface composition and structure of the substrates account for the success or failure of an

adhesive, given that it has the required mechanical properties. For example, Teflon® fluoropolymers are known for their "non-stick" character. Therefore, useful adhesive bonds to these substrates require surface modifications, such as etching with sodium complex solutions[9], recrystallizing against a metal surface, or exposing to an electrical discharge[10]. Similar conclusions were obtained with polyethylene and polypropylene[11], and poly (ethylene terephthalate)[12,13]. It is clear then, that the chemical composition of the surface plays a dominant role in determining the surface properties; i.e. the chemical species present in the outermost few atom layers determine the success of the application of polymers in the areas mentioned. Consequently, information on the chemical composition of surfaces is of primary importance.

Chemical information about surfaces has been classically inferred through physical characterization, using methods such as fluid contact angles and peel testing, that quantify properties that may be related to chemical structure. However, this methods do not provide direct chemical information. Recently, the use of Multiple Attenuated Total Reflectance Infrared spectrometry has greatly improved matters in this direction. Nevertheless, the signals are averaged over a depth of many hundreds of angstroms and a true surface characterization is not

possible yet. More recently still, surface-enhanced Raman spectroscopy has been shown to provide chemical information within a depth scale of 100Å[14]. But, this technique is not routinely available at the present time. Therefore, the surface-sensitive electron and ion spectroscopies based on high vacuum systems are the major candidates for the chemical analysis of polymer surfaces. Furthermore, considering the somewhat fragile nature of organic materials exposed to energetic particles or ionizing radiation, techniques based on the use of an incident beam of photons are the most appropriate ones. That is, the damage induced in a polymer surface by an incident photon beam is less than that caused by electrons or ions. Thus, the vast majority of surface characterizations of polymers has been accomplished using photons as the incident radiation and ejected electron as the detectible species. X-ray Photoelectron Spectroscopy (XPS or ESCA), Ultraviolet Photoelectron Spectroscopy (UPS), and X-ray Auger Electron Spectroscopy (XAES) are the primary surface analysis tools available for polymers. Of these, ESCA is the most widely used due to its versatility and comparative ease of interpretation of the data obtained.

The present work is a study of the surface "orientation" on a series of polymeric materials utilizing X-ray Photoelectron Spectroscopy as the principal probing technique. In other words, the determination of the chemical

composition of the outermost few atom layers was performed and compared to the bulk of the polymers.

In the following sections a review of literature about surface orientational studies performed in polymers is presented. Next, the principles of XPS are discussed before the actual experimental work is reported.

Chapter II

REVIEW OF LITERATURE

The forthcoming review of literature comprises only pieces of work in which surface-orientational studies were performed. Since the introduction of instrumental techniques for the analysis of polymer surfaces, such as XPS, UPS, ISS, an astounding amount of work has been published in the literature. However, not many published investigations are concerned with the preferential orientation of chemical groups at the surface.

In the last few years an important research effort has been made in the biomedical area to study polymer surfaces. Materials for biomedical applications must have good surface properties, e.g. blood compatibility, in addition to adequate bulk properties such as tensile strength, elasticity and fatigue resistance. Segmented polyurethanes were found to be candidates for this application. Two commercially available polyurethanes, Biomer® and Avcothane®, have been subjected to many studies. Biomer® is a polyether urethane with a diamine as a chain extender. On the other hand, Avcothane® is a polyether urethane with a diol as a chain extender, copolymerized with 10% by weight of poly (dimethyl siloxane).

Andrade et al.[15] studied the air-facing and the mold-facing surfaces of Avcothane®. The O/C, N/C, and Si/C relative intensity ratios were used to determine the relative abundances of the different polymer segments at the surface, e.g. hard, soft and siloxane segments. The mold-facing surface was found to be completely covered by siloxane, whereas the air-facing surface (blood compatible surface) was composed of both, polyurethane and poly (dimethyl siloxane). Graham and coworkers[16] found similar results utilizing XPS, SIMS (Secondary Ion Mass Spectroscopy) and ISS (Ion Scattering Spectroscopy). The polyether soft segments and the siloxane segments were more concentrated in the substrate-facing side, and the urethane hard segments were concentrated in the air-facing side. However, ISS, a more surface sensitive technique, revealed that the topmost layers of both sides of Avcothane® contained similar amounts of poly (dimethyl siloxane). Sung et al.[17-19] also investigated Avcothane® surfaces by means of FTIR-IRS (Fourier Transform Infrared-Internal Reflection Spectroscopy), XPS and Auger Electron Spectroscopy. The results were contradictory of those of Graham et al.[16] and Andrade et al.[15] Sung et al. found the air-facing surface of Avcothane® to be covered by poly (dimethyl siloxane) with a small amount of polyether soft segments. The hard segments were not detectable. On the other hand, the substrate-facing

side contained hard segments as well as soft and siloxane segments.

These contradictory results are not surprising given the multicomponent, multiphase nature of these polymers. The bulk and surface properties may be sensitive to such parameters as substrate in contact, rate of evaporation of solvent, temperature, etc. Nyilas and Ward[20] proved the important role of kinetics in surface segregation. These authors determined the effect of the temperature and the rate of evaporation of the solvent on the segregation of poly (dimethyl siloxane) to the surface of Avcothane® using FTIR as the probing technique.

As already mentioned, Biomer® has also been subjected to extensive investigation. Sung and coworkers[17,18], utilizing FTIR and XPS, arrived to the same conclusions as Graham et al.[21] with the aid of XPS, SIMS and ISS. The air-facing surface contained a greater concentration of polyether soft segment than the substrate-facing side. However, this difference in composition was not as prominent as in Avcothane® polyurethane.

Other commercially available polyurethanes have been also subjected to surface studies. Ratner[22] studied Tygothane® (polyester urethane), Superthane® and Pellethane® (polyether urethanes) by means of XPS. In all cases, the surface was found to be enriched with the ester or ether moiety of the polyurethane.

Some non-commercially available polyurethanes have been studied. Stupp and coworkers[23] investigated the effect of the nature of the substrate in which a segmented polyurethane is cast. A polyurethane made of methylene bis (4-phenyl isocyanate), poly (propylene oxide) glycol and p-xylylene diamine cast on poly (ethylene terephtalate) and glass substrates was analyzed by IR-ATR spectroscopy. Surfaces cast on glass substrates showed higher content of polyether, whereas those cast on PET contained higher relative concentration of aromatic segments. The last results were rationalized in terms of hydrogen bonding between carbonyl groups in the substrate and secondary amino groups in the segmented polyurethane, in addition to the aromatic nature of PET chains.

Knutson and Lyman[24-26] examined the effect of molecular and fabrication variables on the chemical and morphological structure of the surface of block copolyether-urethane-ureas. The block copolymers were synthesized from poly (propylene) glycol of various molecular weights, methylene bis (4-phenylisocyanate), and ethylene diamine. With the aid of FTIR and XPS, these authors determined the bulk and surface morphologies. The bulk morphology was found to be a phase separated structure involving essentially complete separated hydrogen bonded urea domains in a polyether matrix. However, a major

interface region connecting the domains of about 10-12Å was observed. On the other hand, the surface showed an enrichment of ether segments and a decrease of the size of the interface region due to decreased mixing between the urethane linkages and polyether matrix close to the surface. Nevertheless, the urea domains remain quite pure on the surface. Another interesting result, obtained by these authors, is the fact that the polyurethane with the highest MW soft segment did not present the highest concentration of ether segments at the surface. On the contrary, polyurethanes containing soft segments with MW = 700, 1000 showed higher concentration of ether segments at the surface than the polyurethanes having soft segments with MW = 2000. These results show the critical importance of the molecular weight of the segments in determining the extent of surface segregation of the components.

Graft-copolymers are, also, good candidates for biomedical applications, since good mechanical and surface properties can be achieved by selecting the appropriate combination of substrate and grafting agents. Ratner et al.[27] studied the effect of hydration and dehydration on the surface composition of several radiation-grafted polymers. Poly (2-hydroxyethyl methacrylate) (HEMA) and poly (acrylamide) grafted onto polyethylene and silicone rubber substrates were investigated using XPS. When grafted to

polyethylene, HEMA and poly (acrylamide) were localized at the surface and they did not undergo changes in graft location upon dehydration. When silicon rubber was the substrate, HEMA and poly (acrylamide) were detected at the surface of the grafted polymer. However, upon dehydration, HEMA and poly (acrylamide) were not detected, being located at an estimated depth of a few hundred angstroms. These results are very important with regard to the implantation *in vivo* of dry radiation-grafted hydrogels, since the surface properties can be different from those of the hydrated hydrogel. This can cause the failure of the implant.

The area of block copolymers has received much attention with regards to the phase separation phenomenon. This phenomenon has been used as a mean to change the surface and bulk properties of polymers.[28,29]

Litt and Matsuda[30] characterized a series of AB block copolymers of poly (N-lauroylethylenimine) (PLI) and poly (N-propionyl ethylenimine) (PPI). Critical surface tension and ATR-IR spectroscopy results indicated a surface covered by long hydrocarbon side-chains of PLI with methyl groups forming a close-packed surface. Approximate Gibbs adsorption isotherms were used to calculate the limiting surface areas of the segments adsorbed at the interface. The comparison of the values obtained, 14-16$\AA^2$/monomer unit, with their previous study of the crystalline structure of PLI[20] led

them to propose a model for the molecular arrangement at the surface. Figure 1 depicts the proposed model. The surface is composed of a 2-dimensional crystalline film with the PLI segments lifted out of the interface, and closely packed hydrocarbon chains at the outermost layer.

A similar study was carried out by Kugo et al.[32] XPS, replication electron microscopy and wettability measurements aided in the elucidation of the surface characteristics of ABA tri-block copolymers of α-helical poly (ε-N-benzyl oxycarbonyl L-lysine) (PBCL) and poly (butadiene) (PB). As expected from surface free energy considerations, PB segregated at the surface of solvent cast films. Electron microscopy showed convex PB domains rising above the planar PBCL matrix. Based on these observations, the authors proposed the model shown in Figure 2 . The presence of interfacial regions between α-helical PBCL and PB in this model was explained in terms of contact angle measurements.

Thomas and O'Malley used angular resolved XPS to study the surface composition and topography of polystyrene (PS)/poly (ethylene oxide) (PEO) diblock[33] and triblock[34] copolymers. The surface composition of the copolymers was found to be richer in PS than the bulk composition. This is not surprising given the lower critical surface tension of PS, 36 dyn/cm as opposed to 44 dyn/cm for PEO. Furthermore, PEO can crystallize at room temperature. A comparison of the

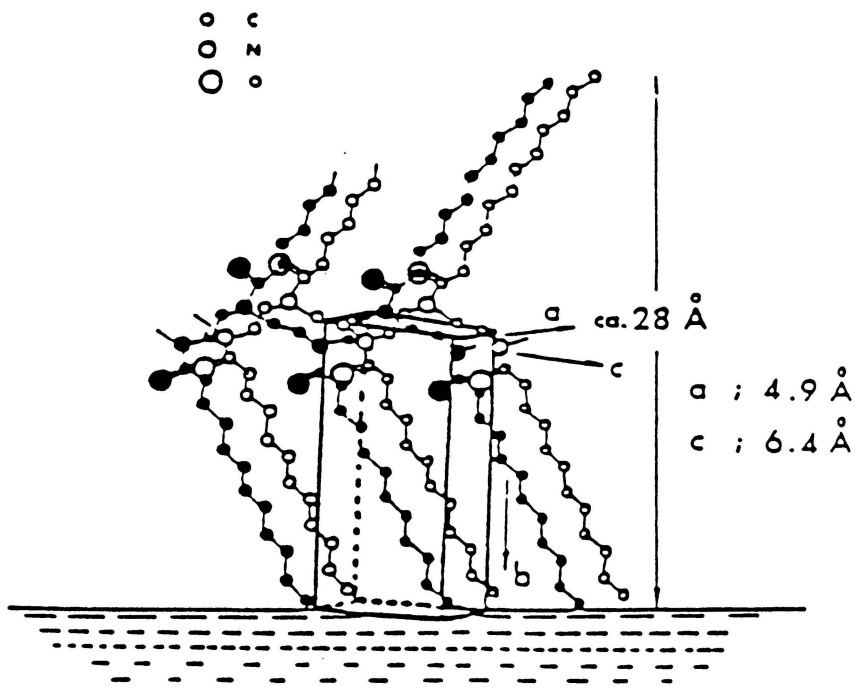

Figure 1: Schematic representation of packing of PLI molecules at the solution/air interface. [from 30]

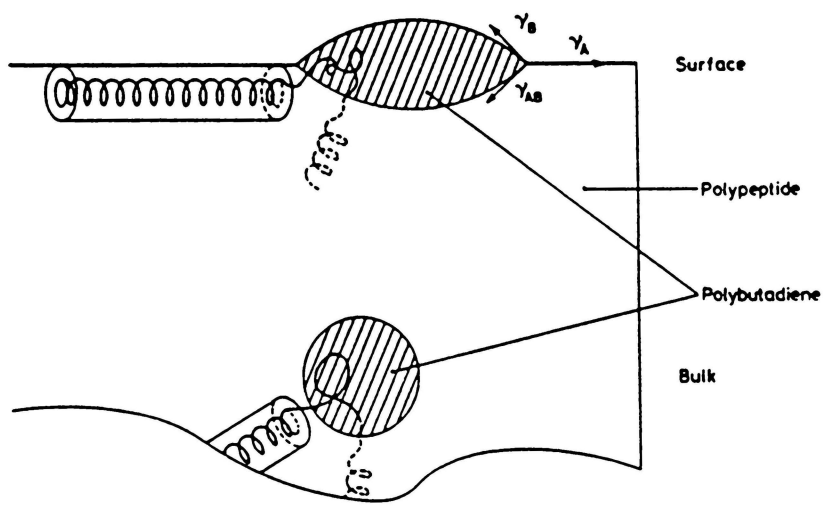

Figure 2: Schematic representation of cross-sectional model for the PBCL/PB/PBCL copolymer.[from 32]

theoretical angular dependent intensity functions to the experimental data led to propose a surface model with non-planar topography as model d) in Figure 3. This investigation also showed that partial miscibility occurred in the surface region as a result of some electronic interactions between the PEO and PS blocks.

Clark et al.[35] investigated the surface morphology of AB block copolymers of poly (dimethyl siloxane) (PDMS) and polystyrene (PS) by XPS and contact angle measurements. Copolymers containing 23% and 59% wt. of PS were studied. Given the differences in the solubility parameters of the two components (PDMS = 7.3 and PS = 9.1)[36] and the lower critical surface tension for PDMS (PDMS = 22 dyne/cm versus PS = 33 dyne/cm)[37], PDMS was expected to phase segregate to the surface. Indeed, that was the case. Critical surface tension and XPS data indicated a surface overlayer of PDMS in both copolymers. The estimated layer thickness varied between 13Å and 40Å depending on the method of formation of the film. Thomas and O'Malley[38] obtained similar results when studying random block copolymers of poly (hexamethylene sebacate) (PHMS)/poly (dimethyl siloxane) (PDMS). However, PDMS did not totally dominate the surface layer even at PDMS bulk concentrations as high as 72.5% wt.

McGrath et al.[39] and Dwight and coworkers[40] examined perfectly alternating poly (bisphenol-A carbonate) (PC)/PDMS

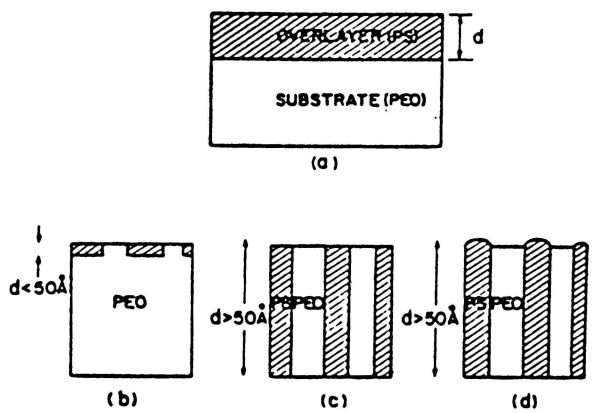

Figure 3: Schematical representation of models for the surface topography of the PS/PEO copolymers. [from 33]

and PC/polysulfone (PSF) with the help of XPS. In both cases, the lower surface free energy component dominated the surface, i.e. PDMS in the PC/PDMS copolymer and PC in the PC/PSF system. Riffle[41] examined PDMS/PC copolymers of various block lengths by means of XPS. The block length was the governing factor in determining the surface composition rather than the bulk composition. Keeping the siloxane block length at 1800g/mole and varying the siloxane weight percentage from 11% to 40% produced surfaces of similar composition (about 60% w/w siloxane). Whereas, when the block length was increased to 5000g/mole and 10000g/mole, each of approximately equal composition, surfaces of 82% and 92% siloxane were, respectively, obtained. An interesting behaviour was observed when the copolymer of 1800g/mole siloxane block was blended with PC homopolymer. PDMS was seen in considerable amounts (ca. 10%) at the surface even at bulk concentrations as low as 0.05%wt. siloxane. A very well defined break in the surface concentration of PDMS was observed at about 1% PDMS in the bulk. At this bulk composition, the surface content of PDMS jumped to a value above 65% wt. Sha'aban[42,43] obtained similar results investigating block copolymers of poly (ether urethane) Estane® and PDMS by means of XPS. A model for the surface was postulated considering the relative surface free energies of the three different components. The topmost

layer would be covered by PDMS, followed by a layer of polyether segments and, finally, a layer of highly H-bonded polyurethane hard segments.

Patel[44] investigated surface and bulk composition and morphology of siloxane containing block copolymers and their blends. XPS and Transmission Electron Microscopy (TEM) were used in the study. Poly (bisphenol-A sulfone), poly (aryl ester), poly (urea) and poly (imide) in block cooplymers with PDMS were analyzed. In all cases, an uniform siloxane rich layer was found at the surface. Whereas, the bulk had microphase separated domain structure. The blends of block copolymers with PDMS presented pronounced siloxane enrichment at bulk concentrations as low as 0.05%wt. siloxane. The molecular weight of the blocks in the copolymer was found to be a very important parameter governing surface and bulk properties in the copolymers as well as the blends.

Homopolymer blends have also been investigated, with special applications in the coatings industry. Phillips and coworkers[45] studied the effect of coating thickness or surface to volume ratio on the surface chemical composition of blends. Binary blends of polymers of general structure $F(CF_2)_n$-$(CH_2)_2OOC$-$[C(CH_3)$-$CH_2]_x$ were analyzed. The fluoroalkyl chain length was varied in the polymers. Interesting results were obtained when the surface was

probed by XPS. The surface composition was found to be dependent on the surface/volume ratio or thickness of the film. For thicknesses above 1μm or $S/V<10^{4}cm^{-1}$ the coating surface was essentially composed by the polymer with longer fluoroalkyl side-chain. Whereas, for thicknesses below 1μm or $S/V>10^{5}cm^{-1}$ the surface was essentially covered by the polymer with shorter fluoroalkyl side-chain.

In the pieces of work discussed so far, angle-resolved XPS was used directly on the copolymers. However, in some cases, chemical derivatization of the surface groups needs to be done in order to differentiate them from the rest of the molecular structure. Dickie et al.[46] characterized methyl methacrylate (MMA) - hydroxypropyl methacrylate (HPMA) copolymers using angular dependent XPS in conjunction with trifluoroacetic anhydride derivatization. XPS results, after derivatization, indicated a preferential orientation of the fluorine containing moieties away from the specimen surface into the bulk of the polymer. The results were consistent with an initial preferential orientation of hydroxyl groups away from the surface. A multilayer model for the surface with 0.2nm thick layers was proposed. The outermost layer was a hydrocarbon backbone, followed by a layer containing C and O, and finally a layer composed of C,O and F. Figure 4 shows a schematic illustration of the molecular dimensions of the model.

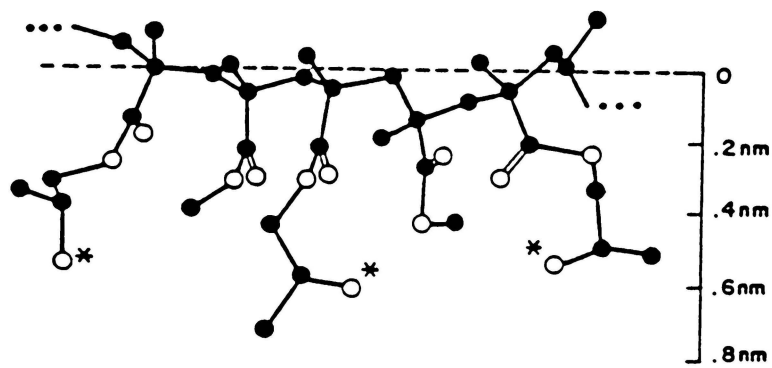

Figure 4: Schematic illustration of molecular dimensions in MMA/HPMA copolymers.[from 46]

A different kind of study involves the investigation of surfaces of homopolymers to determine the chemical groups present in the outermost few atom layers. Gardella et al.[47] investigated changes in the morphology of poly (tetramethyl-p-silphenyl siloxane) (pTMpS). XPS and FTIR results were correlated to thermal (DSC) and crystallographic data. FTIR and XPS data indicated that as sample crystallinity increased in pTMpS, the surface oxygen content decreased. The polymer crystal surface is presumed to be comprised of loops or folds where the disorder is greater than that found in the crystalline core material[48]. Therefore, the data indicated a higher concentration of Si-O linkages found at the interfacial folds or loops of spherulitic lamellae. That is, the presence of surface segregated Si-C_6H_4-Si-O linkages in the form of folds or loops of the long chains going back into the rod-like crystalline core of the material. This hypothesis was confirmed using hydrofluoric acid etching, that etched away the less ordered surface material and increased relative sample crystallinity[49]. Indeed, the same results were obtained following the etching by XPS, FTIR and DSC measurements.

Chapter III

X-RAY PHOTOELECTRON SPECTROSCOPY

A REVIEW

In the following sections a discussion of the physical phenomena taking place in this analytical technique and the information that can be obtained is carried out.

PHYSICAL ASPECTS

X-ray Photoelectron Spectroscopy (XPS), commonly known as ESCA (Electron Spectroscopy for Chemical Analysis) comprises the irradiation of a sample with monoenergetic x-rays and analysis of the electrons emitted. Figure 5 shows the photoelectric process that takes place when a material is irradiated with x-rays.

The electrons emitted from the sample have different kinetic energies. These values depend on the atomic environment, the energy of the incident x-ray beam, and the spectrometer work function. The kinetic energy of the emitted electrons can be expressed as

$$KE = h\nu - BE - \phi \qquad (3.1)$$

where $h\nu$ is the photon energy, BE is the binding energy of the atomic orbital from which the electron is ejected, and ϕ is the spectrometer function. Thus, with a knowledge of the

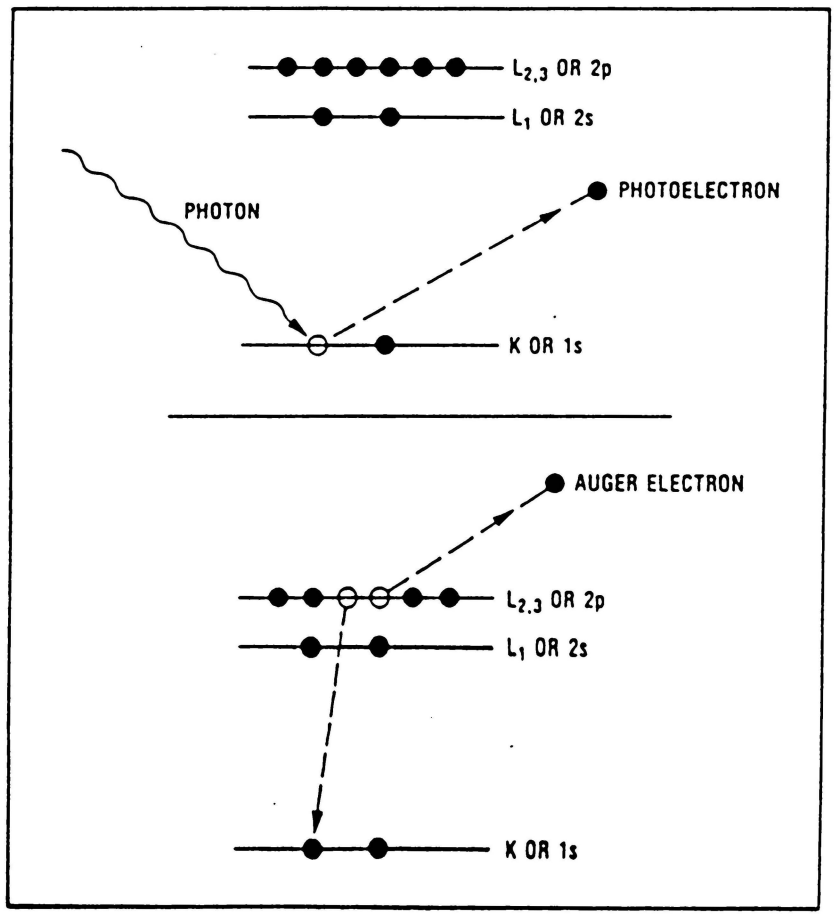

Figure 5: Photoelectron and Auger processes. [from 51]

photon energy, measuring the kinetic energy of the photoemitted electrons, XPS provides a technique to determine the binding energies of, in principle, all electrons from the core to the valence levels. Hydrogen and helium are two exceptions since core and valence energy levels are not distinguishable for these two species.

It has been already stated that x-ray radiation is used as the excitation source. The most commonly used lines are the $AlK\alpha_{1,2}$ ($h\nu$=1486.6eV.) and $MgK\alpha_{1,2}$ ($h\nu$=1253.6eV.) radiations, that are emitted by aluminum and magnesium when the metals are bombarded with high energy electrons. These $K\alpha_{1,2}$ radiations are relatively "soft", in the sense of their low photon energy. Ocassionally, x-rays of higher energy have been used as $CuK\alpha_{1,2}$ ($h\nu$=8048eV.), $CrK\alpha_{1,2}$ ($h\nu$=5415eV.), and $TiK\alpha_{1,2}$ ($h\nu$=4511eV.).[52]

In addition to the photoelectric process, relaxation processes (de-excitation of the hole state) occur within a time scale of 10^{-13}-10^{-14} seconds. The relaxation processes can take place by means of x-ray fluorescence and Auger processes.

The Auger emission process can be considered a two step process. First, the ejection of an electron from an inner shell by an impinging photon. Then, an electron falls from a higher level to the vacancy in the inner shell, with simultaneous ejection of a second electron. The process is

shown in Figure 5. The kinetic energy of the Auger electron is equal to the difference between the energy of the initial ion and the doubly-charged final ion. This means that the kinetic energy of the Auger electron is independent of the mode of initial ionization. The Auger process gives rise to another spectroscopic technique, namely Auger Electron Spectroscopy (AES). C.D.Wagner has reviewed the subject.[53]

The emission of x-rays, as a relaxation process, can also be used as a means of qualitative analysis (Secondary Emission Analysis)[50]. Figure 6 shows a plot of the x-ray fluorescence yield and Auger electron yield as a function of atomic number for the light elements in the periodic table.

Two other processes can also take place, i.e. shake-up and shake-off processes arising from valence level transitions accompanying core-level photoemission. A fair description of these processes is given in further sections.

The exciting photons can penetrate deeply into the sample to excite electrons. These electrons (photoelectrons) travelling through the material have a relatively high probability of experiencing inelastic collisions with bound electrons, suffering energy losses. If these inelastic scattering processes occur frequently, the photoelectron flux emerging from the sample will be attenuated. This effect is extremely important in solids, where photoelectrons can scape only from a very short distance

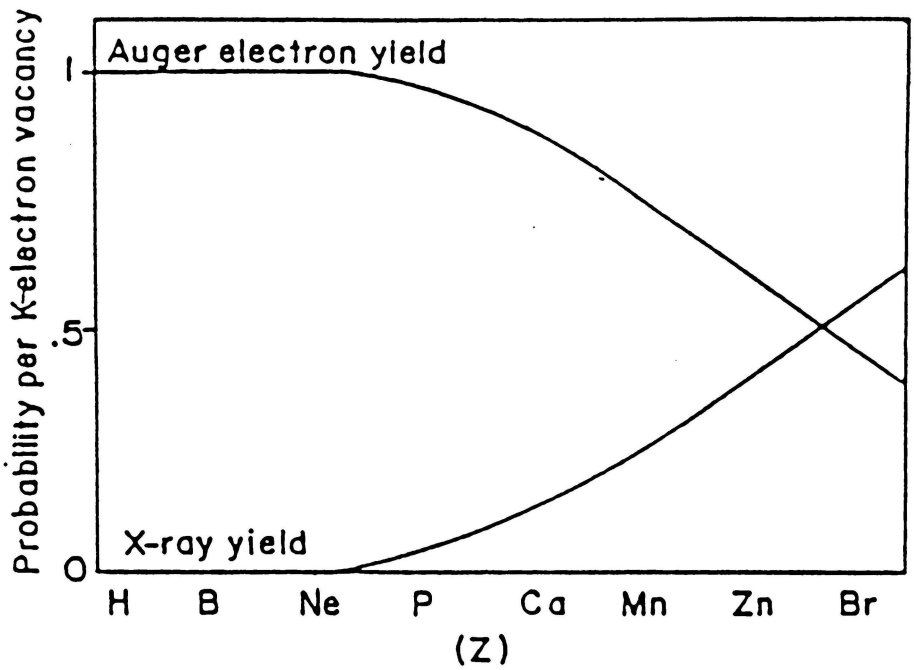

Figure 6: Diagram of x-ray fluorescence and Auger electron yields vs. atomic number.[from 54]

underneath the surface (typically in the range of tens of angstroms). The exact probing depth depends on the solid surface morphology and chemistry, as well as the kinetic energy of the photoelectrons. This fact gives the technique its surface sensitivity and provides a means of differentiating surface from sub-surface and bulk phenomena.

The attenuation of the photoelectron flux mentioned above leads to the concept of inelastic mean free path, mean scape depth or attenuation length λ of an electron of energy E in a certain material. It represents the depth from which 1/e of the photoelectrons produced can scape. Further discussion of the mean free path is given in following sections.

CHARACTERISTICS OF THE SPECTRA

After having discussed some of the phenomenological highlights of XPS, an overview of the nature of the spectrum that can be obtained will be given.

The spectrum is displayed as a plot of electron kinetic energy vs. the number of electrons in a fixed energy interval. Due to the complexity of the processes that take place, the spectrum presents many kinds of lines, namely photoelectron lines, Auger lines, shake-up lines, shake-off lines, and valence bands.

Core Energy Level Photoelectron Lines

The photoelectron lines are usually symmetrical, and are typically the narrowest lines present in the spectrum, unless more than one species is present under the same envelope. The peak width is a convolution of the natural line width, the width of the exciting x-ray line and the instrumental contribution to it. Photoelectron peaks can be obtained from all the elements of the periodic table except H and He. The photoelectron lines are sufficiently unique for elemental identification, although a few problems of overlap do exist. But, in most cases the presence of more than one peak with reasonable intensity in elemental core level spectra helps overcoming the problem.[55]

The core levels are essentially localized in atoms. Their energies are characteristic of the given element. However, they are sensitive to the electronic environment of the atom. Therefore, for a given core level of a given element, differences in the electronic environment of the atom in a molecule give rise to a small range of binding energies, i.e. "chemical shifts". These "chemical shifts" are often representative of a particular structural feature. Therefore, the chemical state of the elements may be recognized by measuring the exact peak position. Figure 7 shows two chemical states of Germanium on a Ge3d and a Ge2p spectra.

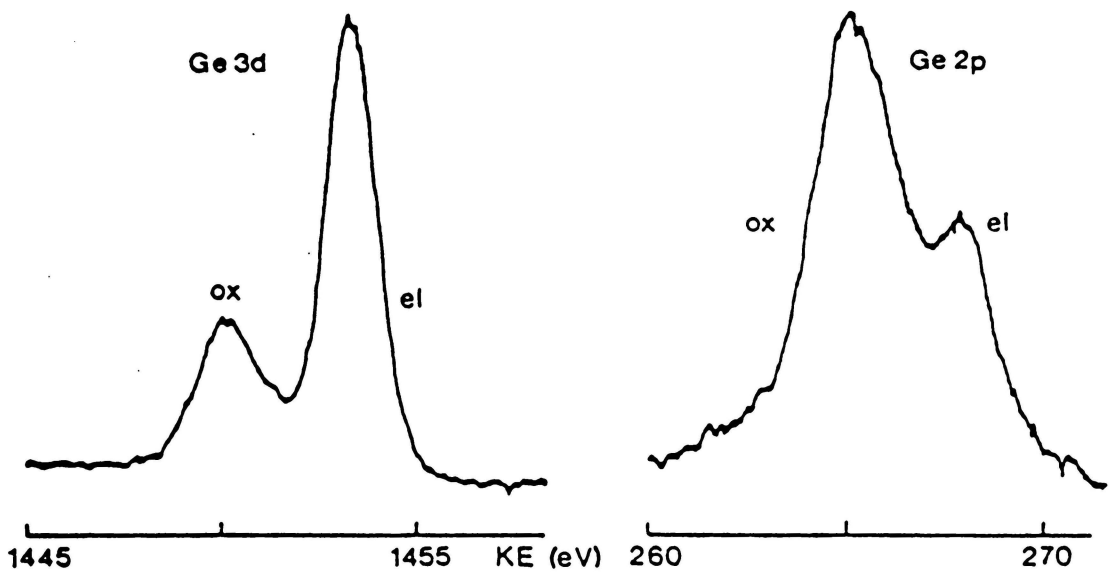

Figure 7: Ge core level spectra from Ge metal with a passive oxide overlayer. Two chemical states of Ge, Ge(0) and Ge(IV) can be observed.[from 56]

As stated previously, the binding energy of the primary photoelectron is directly related to its kinetic energy. Tables of core electron binding energies have been compiled by Siegbahn et al.[57]

Auger Lines

Auger lines are groups of lines in rather complex patterns produced by a relaxation process. Since Auger lines have kinetic energies that are independent of the ionization radiation, they appear on a binding energy plot to be in different positions when ionizing photons of different energy are used. Until recently, these peaks were not of importance as analytical tools. However, Wagner[53] has pointed out the advantages of using the separation between principal Auger and photoelectron peaks as an analytical parameter which is independent of charging effects (the Auger parameter α).

Shake up and Shake off Processes

Another level of information, not very exploited yet, is the shake up and shake off phenomena. As a result of a vacancy formed in a given orbital due to photoionization, electrons see a change in the effective nuclear charge due to an alteration in the electron screening. This change in effective charge is a sufficiently large perturbation to

cause simultaneous excitation of a valence electron from an occupied to an unoccupied level (shake up) or ionization of a valence electron (shake off) in addition to main photoionization[58-60]. Figure 8 pictures these processes.

Manne and Åberg[61] have established the theoretical relationship between shake up and shake off processes and relaxation energy. They have shown that the weighed average of the energy of each of the events, direct photoionization, shake up and shake off, corresponds to the binding energy of the unrelaxed system. For C1s levels the relaxation energies fall in a narrow range, e.g. 12eV[62]. Therefore, it can be shown that shake up and shake off phenomena are generally occurring events. However, when studying solids, shake up and shake off peaks are masked by a general tail arising from inelastic events. Only systems presenting relatively high intensity low energy shake up satellites are appropriate for obtaining information. In particular, unsaturated systems invariably present satellites of appreciable intensity in the region up to ~12eV that are attributable to $\pi \rightarrow \pi^*$ transitions.

Despite their importance, shake off transitions do not seem of general applicability for analysis of polymeric systems. On the contrary, the interpretation of low energy shake up satellites broadens the scope of XPS. The shake up structure is characteristic of the higher occupied and lower

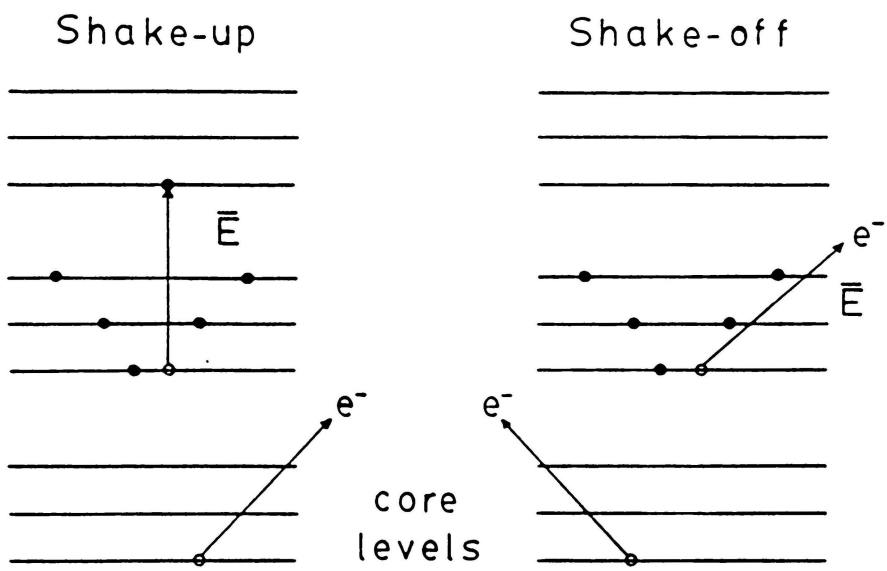

Figure 8: Diagrams of shake up and shake off processes.

unoccupied valence orbitals. Therefore, shake up satellites may be used to fingerprint molecular systems when direct photoionization peaks for two compounds are identical. This is, especially, the case of purely hydrocarbon polymers, in which useful information concerning structure and bonding can be obtained. Clark and Dilks[63,64], as well as Clark and coworkers[65] have undertaken a systematic investigation of shake up phenomena in polymeric materials. Figure 9 illustrates some of the results obtained by Clark and Dilks[64] for a series of polystyrenes in which a para substituent is introduced. The different band shapes of the shake up peaks are noted when changing from polystyrene to poly(p-methylstyrene) and to poly(p-t-butylstyrene).

Although very detailed and sophisticated analysis of shake up structures can be done[64], the practical applications involve the measurement of relative intensities and overall band profiles rather than specific assignment of the transitions.

Valence Energy Level Bands

In the previous sections, emphasis has been placed on the study of the core levels of polymeric systems in which information concerning structure and bonding has been inferred from shifts in core binding energies. In this section, the valence energy levels of polymers are discussed.

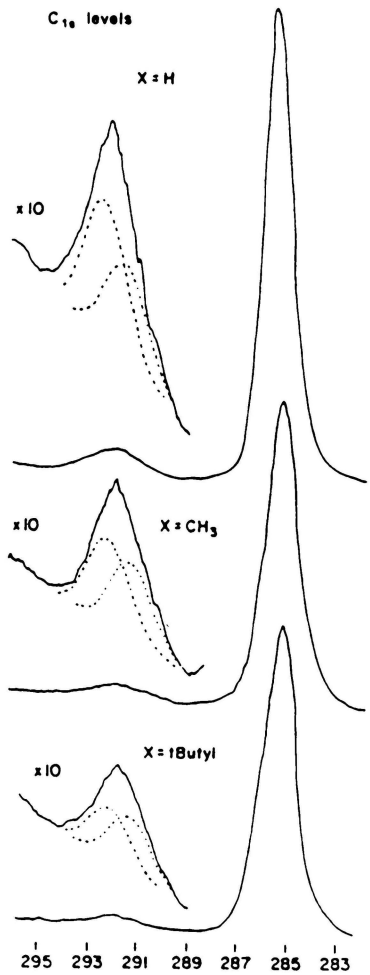

Figure 9: Core level spectra of polystyrene, poly(p-methyl styrene), and poly(p-t-butylstyrene).[from 64]

The valence bands include the less bound electrons, those that are directly involved in the bonds between the atoms of the molecule. Therefore, even if very low cross-sections characterize these low energy electrons, the valence band spectra provides useful, and in many cases unique information compared to the core level lines. However, the recording of polymer valence band spectra requires very careful and patient experimentation.

Similar to the core levels, a valence band photoelectron spectrum is composed of peaks or bands having characteristic binding energy, intensity, peak or band width and shape. Nevertheless, the interpretation of the data necessitates the support of elaborate and accurate quantum mechanical calculations or the comparison with other types of experimental data, in order to extract the maximum of information.

The materials that have received most attention, as far as valence band spectra is concerned, are the homopolymers of ethylene and fluoroethylenes[66]. Figure 10 shows experimentally obtained valence band spectra for polyethylene and a series of polyfluoroethylenes. Alongside, the same spectra theoretically calculated are displayed. The tight binding crystal orbital method LCAO-CO with a basis set of valence atomic orbitals was used in these calculations. The similarity of the experimental and theoretical spectra is remarkable.

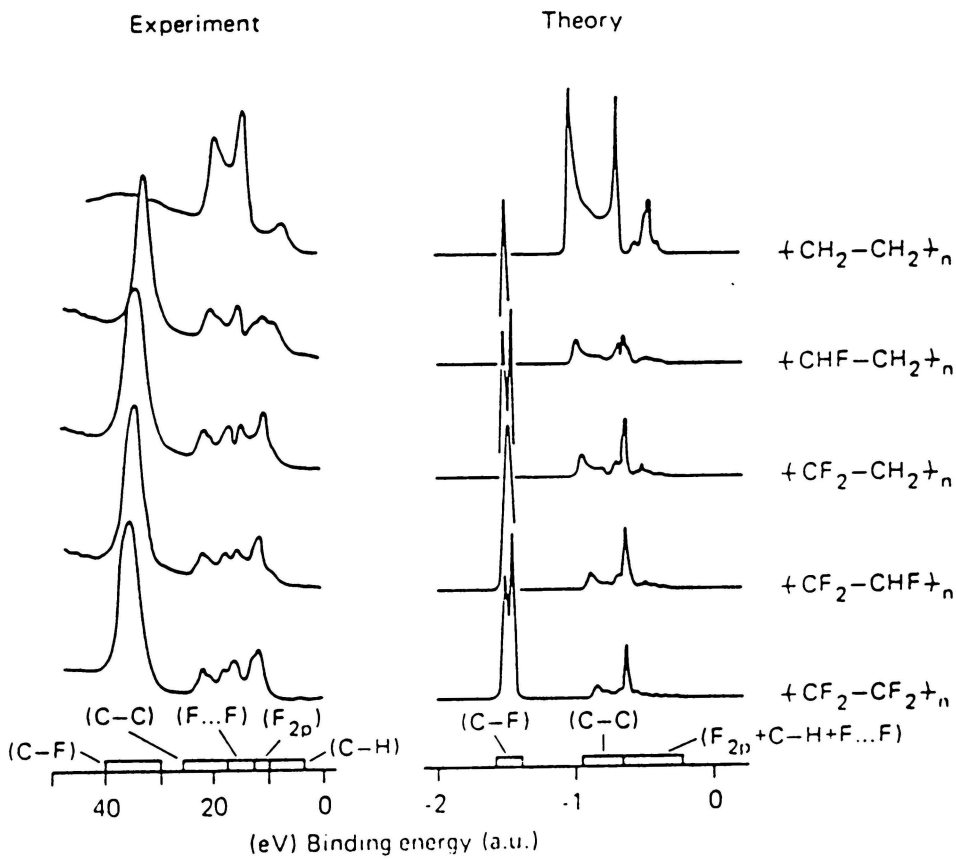

Figure 10: Experimental and theoretical valence band spectra of a series of fluoropolymers. [from 66c]

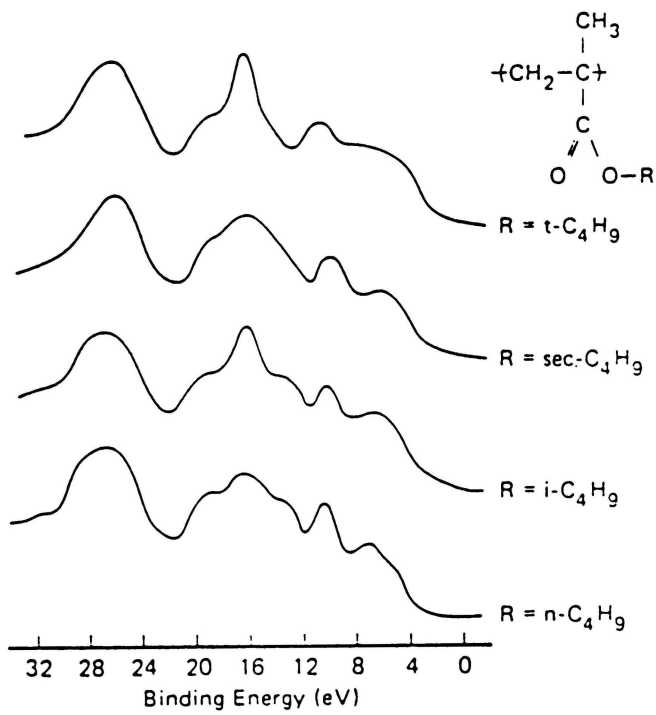

Figure 11: Valence band spectra of the isomeric poly (butyl methacrylates).[from 68b]

Pireaux et al.[67] have proved that the XPS valence band, in conjunction with quantum mechanical calculations allows one to obtain information on the alternating or block structure of an ethylene-tetrafluoroethylene copolymer. Clark and Thomas[68] have shown the unambiguous assignment of structural isomerism on a series of polyacrylates and polymethacrylates. Figure 11 depicts the valence band spectra of a series of isomeric poly (butyl methacrylates).

Pireaux et al.[69] have demonstrated that valence band spectra, like core level shake up spectra, allows one to distinguish between saturated and unsaturated hydrocarbon polymers, e.g. polystyrene and poly (vinyl cyclohexane). Stereoisomerism has also been probed. Cis and trans isomers of poly(isoprene) with short branched chain and small substitution effects do not show significant differences. However, isotactic and syndiotactic polypropylene revealed valence band spectra profoundly different by their C2s band shape.[70,71]

For an interesting review of valence band spectra of polymers, Pireaux et al.[72] is suggested.

ENERGY REFERENCING

This section is devoted to the discussion of surface charging effects and consequent energy referencing.

The photoelectric process that generates the XPS spectrum leaves the surface positively charged. If the material is an insulator -as the case of polymers- electrons can not flow to neutralize that charge, and the sample remains positively charged. Therefore, the kinetic energy of the electrons leaving the charged surface is given by

$$KE = h\nu - BE - \phi - Q \qquad (3.2)$$

where KE is the kinetic energy, $h\nu$ is the incident photon energy, BE is the binding energy of the electrons, ϕ is the spectrometer work function and Q is the sample charge. This means that the binding energy scale will be shifted an amount equal to Q, which is material dependent. However, it should remain constant for a given sample during the analysis. Surface charging is also dependent on the length of time the sample is probed with x-rays.

The distribution of charge on the surface of insulators can also cause a broadening of the photoelectron line width which can represent problems when resolving doublets or shoulders. There are several experimental methods to deal with the sample charging effects to obtain the true binding energy of the photoelectron being analyzed [73]. The most

frequently used method consists of the utilization of internal standards. The method of standardization consists of taking a photoelectron line whose true binding energy is known and substracting the measured binding energy to determine the amount of shift due to sample charging. This shift factor is used to correct the measured binding energy values of all other photoelectron lines in the spectrum. For polymers, the C1s photoelectron line corresponding to hydrocarbon at BE=285.0eV is the most frequent reference, even though the value is still under discussion.[74]

QUANTITATIVE ANALYSIS

Not only qualitative, but also semiquantitative information can be acquired from XPS surface analysis. Three approaches have been proposed for the quantitative analysis of surfaces, namely standards, elemental sensitivity factors, and first-principles model.

The first approach involves the use of a number of reference standards with compositions encompassing those that are likely to be encountered in practice. This method is useful when samples with a limited range of composition are to be routinely analyzed.

The use of elemental sensitivity factors for surface analysis was extensively studied by Wagner[75,76] and by Jörgensen and Berthou[77]. These authors developed a relative

intensity scale from which the elemental sensitivity factors were determined with reference to the F1s peak intensity. Therefore, calculations can be performed utilizing the following equation,

$$N_1/N_2 = [I_1/a_1]/[I_2/a_2] \qquad (3.3)$$

where N_i is the atomic density of species i, I_i is the intensity measured in the XPS experiment and a_i is the sensitivity factor for the i species referenced to F1s.

The first-principles model approach relates the observed intensity to basic material properties and to experimental conditions by means of x-ray bombardment, photoelectron creation, transport of photoelectrons to the surface and detection. Detailed studies of various situations in terms of the first-principles model are discussed by Fadley[78], Palmberg[79], Ebel at al.[80], Fadley and coworkers[81], and Bishop et al.[82]

Figure 12 shows an idealized sample-spectrometer geometry that is used for calculating photoelectron peak intensities from solid specimens. With the help of this figure, a general expression for the number of photoelectrons produced by subshell k can be written

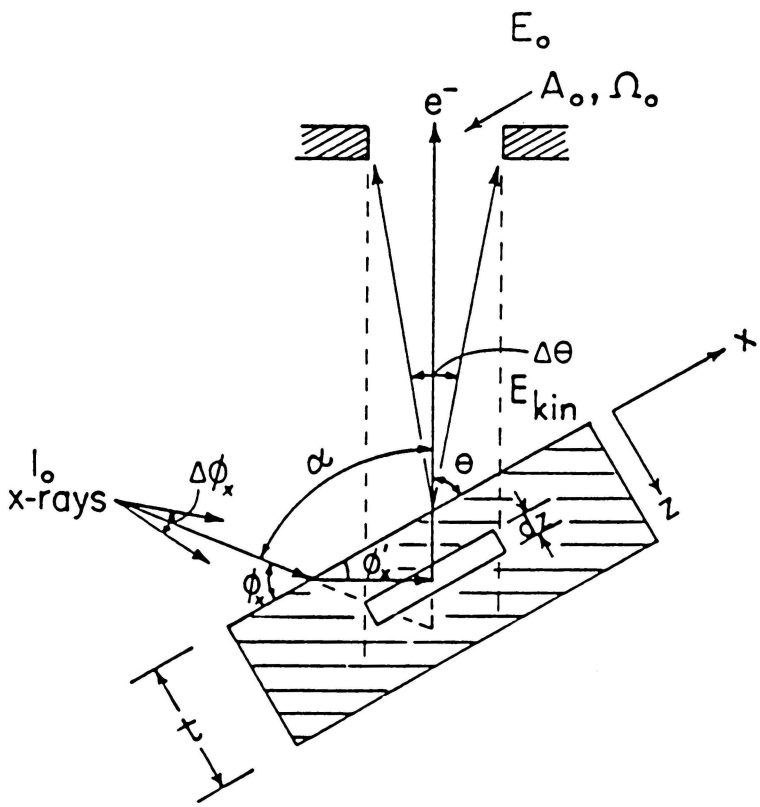

I_o = intensity of oncoming x-rays
A_o = area of spectrometer entrance aperture
Ω_o = geometrical solid angle of acceptance of the spectrometer
E_{kin} = energy of the electrons off the sample surface
E_o = energy of electrons in the analyzer after retardation
$\phi_{x'}, \phi_x$ = x-ray incident and refraction angles at the sample surface
θ = average electron exit angle
α = angle between the oncoming x-rays and exciting electrons
$\Delta\phi_x, \Delta\theta$ = maximum uncertainty in ϕ_x and θ respectively

Figure 12: Idealized spectrometer geometry to calculate photoelectron peak intensities from solids. [from 83]

as follows:

$$dN_k(\theta) = \begin{bmatrix}\text{x-ray flux}\\ \text{at depth}\\ z\end{bmatrix} \cdot \begin{bmatrix}\text{number of}\\ \text{atoms in}\\ \text{volume}\end{bmatrix} \cdot \begin{bmatrix}\text{probability for}\\ k \text{ emission}\\ \text{into } \Omega_o\end{bmatrix}$$

$$\cdot \begin{bmatrix}\text{fraction}\\ \text{escaping in}\\ \text{no-loss peak}\end{bmatrix} \cdot \begin{bmatrix}\text{intensity loss}\\ \text{factor due to}\\ \text{retardation}\end{bmatrix} \cdot \begin{bmatrix}\text{detection}\\ \text{efficiency}\end{bmatrix} \tag{3.4}$$

or,

$$dN_k(\theta) = \{I_o[1-R][\sin\phi/\sin\phi']\exp[-z/\lambda_x\sin\phi']\}$$

$$\cdot\{\rho[A_o/\sin\theta]dz\}\cdot\{[\mu\sigma_k/\mu\Omega]\Omega\} \tag{3.5}$$

$$\cdot\{\exp[-z/\lambda_e(E)\sin\theta\}\cdot\{FE_o/E\}\cdot\{D_o\}$$

where $dN_k(\theta)$ is the number of photoelectrons produced by subshell k as a function of the electron take off angle θ, R represents the x-ray reflection coefficient, ρ is the number density of the atom under consideration, λ_x and λ_e are the mean free paths for x-rays and electrons respectively, $\partial\sigma_k/\partial\Omega$ is the differential cross-section for the k subshell, $F(E_o/E)$ and D_o represent, respectively, a function describing the intensity loss caused by retardation and overall detector efficiency.

Considering a homogeneous sample of atomically flat surface and infinite thickness, Equation 3.5 yields a simpler form after integration:

$$N_k = A\rho[\partial\sigma_k/\partial\Omega]\lambda_e(E)T(E) \qquad (3.6)$$

with A being a factor accounting for the sample/spectrometer geometrical configuration and T(E) the spectrometer transmission function.

Writing Equation 3.6 for the l subshell of a different atom and taking the ratio give rise to the widely used concept of intensity ratios,

$$\frac{N_k}{N_l} = \frac{\rho_1[\partial\sigma_k/\partial\Omega]\lambda_e(E_1)T(E_1)}{\rho_2[\partial\sigma_l/\partial\Omega]\lambda_e(E_2)T(E_2)} \qquad (3.7)$$

In further sections, a brief description of the differential cross-section for k subshell $[\partial\sigma_k/\partial\Omega]$, the electron mean free path $\lambda_e(E)$ and the spectrometer transmission function T(E) is given.

Differential Cross Section

As the photoelectron emission is not isotropic in nature, spatial and directional anisotropies can occur which cause a dependence of the cross section for photoionization on the angle α between the directions of the incident x-rays and the ejected photoelectrons. The relationship of the

differential cross section to the angle α can be expressed as follows[76],

$$[\partial\sigma_k/\partial\Omega] = \sigma_k\{1 + 0.5\beta[1.5\mathrm{Sin}^2\alpha - 1]\} \qquad (3.8)$$

where σ_k is the total cross section for photoionization, and β is the asymmetry parameter. Calculations of σ_k for levels of the elements that can be excited by Kα lines of magnesium and aluminum have been done by Scofield[84] and Nefedov et al.[85], and experimentally verified by Wagner et al.[76] The asymmetry parameter β is a function of the particular level and the energy of the impinging x-rays. Reilman et al.[86] have calculated values of the assymetry parameter for aluminum and magnesium Kα x-rays and the atomic levels that can be photoionized by these sources. Its value varies from -1 to 2, being 2 the value for the s levels.

Electron Mean Free Path

The electron mean free path is dependent on the kinetic energy of the electron and the properties of the matrix through which it travels. C.J.Powell[87] has reviewed the work done in this area. Since this rewiew, a great amount of experimental and theoretical investigation has been published in the literature. Penn[88] has theoretically calculated λ(E) for free-electron-like materials. The

relationship proposed by Penn, valid for electrons of E>200eV is as follows,

$$\lambda(E) = E/\{a[\ln E + b]\} \quad (3.9)$$

where a and b are constants characteristic of the particular material. The values calculated with this equation are believed to be accurate to about 5%.

Some investigators have used a simple power law,

$$\lambda(E) = KE^{n} \quad (3.10)$$

to describe the variation of the mean free path as a function of electron energy. In this equation K is regarded as a constant characteristic of the material. The value of the exponent n has been estimated from fits to experimental data and values in the range 0.50-0.85 have been proposed.

Seah and Dench[89] have made a compilation of the data published up to that time and have determined a value of n=0.50 for electrons with E>150eV. Wagner et al.[90] have determined values of n higher than 0.50 from different sets of data. Values in the 0.65-0.75 range for the 150-4000eV energy range were determined. Later, Szajman[91,92] calculated an energy dependence of the mean free path from a modification to the dielectric theory. The proposed value for the exponent was 0.75 for electrons with energy higher than 300eV. Recently, Ashley and Tung[93] calculated n for

electrons in the energy range 400-2000eV, determining a range from 0.65 to 0.80 for different solids. These authors also stated the dependence of n on the material.

Transmission Function

The transmission function of a spectrometer accounts for the intensity loss caused by retardation and overall detector efficiency. Most commercial XPS instruments have electrostastic deflection-type analyzers to disperse the electrons. Kuyatt[94] determined that for this type of analyzers, the transmission function $T(E_a)$ is a linear function of electron energy in the analyzer E_a.

Normally, spectrometers employ pre-retardation of electrons before energy analysis in order to improve resolution[95]. This is based on the principle that electrons can be accelerated or retarded without changing their absolute energy spread. Two modes of retardation are used, namely Fixed Retardation Ratio (FRR) and Fixed Analyzer Transmission energy (FAT). In the FRR mode, the analyzer operates at a constant resolving power since all electrons are retarded by the same ratio. Therefore, as $T(E_a)$ is proportional to E_a, the transmission function T(E) is also proportional to the electron energy (E) before retardation. On the other hand, in the FAT mode the analyzer transmission energy (E_a) is mantained constant, independent of the energy

of the oncoming electrons. Consequently, T(E) is independent of electron energy(E). Hughes and Phillips[96] found these relationships to be valid, both theoretically and experimentally.

Angle-dependent Depth Profile

A surface sensitivity enhancement can be obtained by decreasing the angle between the surface of the sample and the normal to the acceptance slit of the analyzer as shown in Figure 12. It was first pointed out by Fadley and Bergström[97] that surface-atom relative intensities could be increased by approximately one order of magnitude for grazing angles of electron escape. Subsequent XPS investigation by Fraser et al.[98] provided a more quantitative model for analyzing low-angle distribution measurements. The subject has been extensively explored by Fadley.[78]

Equation 3.11 shows that the fraction of electrons escaping with no loss of energy is proportional to an exponential function of the depth the electron travels,

$$\text{No loss fraction} \propto \text{Exp}[-z/\lambda(E)\text{Sin}\theta] \qquad (3.11)$$

Therefore, variation of the photoelectron "take off" angle, as shown in Figure 13, allows one to effectively perform analysis of a sample at different depths.

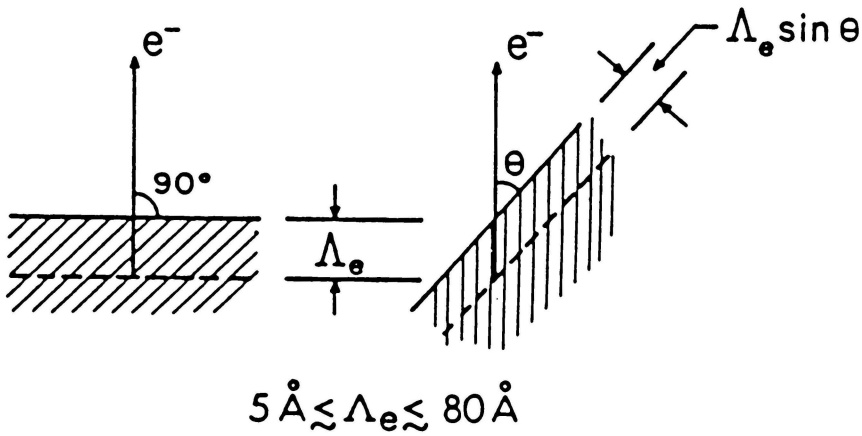

Figure 13: The basic mechanism producing surface enhancement for low electron exit angles. [from 78]

Semiquantitative relative atomic fractions as a function of the "take off" angle can be calculated using Equation 3.7. More accurate calculations can be performed by postulating surface models in terms of concentration profiles, predicting the intensity function by integration of Equation 3.5, and comparing it to the experimental values until the best fit is obtained. This method was employed by Clark et al.[99] and Paynter[100] for flat surfaces. When rough surfaces are considered, the models get very complicated since shadowing of oncoming x-rays and emerging photoelectrons can occur. A deep analysis of this matter was done by Fadley et al.[79]

Chapter IV

EXPERIMENTAL

MATERIALS

The materials used in this investigation can be gathered into four groups:

- Poly (ethylene terephthalate).
- Block co-polyesters and polyesters.
- Fluorine containing polymers.
- Polyurethanes.

Poly (ethylene terephthalate) of different degrees of crystallinity (22%, 29%, 39%, 51%) were obtained from Prof. G.L.Wilkes' characterization laboratory at Virginia Tech, Blacksburg, Virginia. The block co-polyesters , as well as the homo-polyesters for the second group were acquired from Prof. M.L.Polk's synthesis laboratory at Atlanta University,Georgia. Tables 1 and 2 show the structures and names of the block co-polyesters and homo-polyesters used[101-103]. The third group was comprised by poly (chloro trifluoro ethylene) (PCTFE) and (chloro trifluoro ethylene) (CTFE) / ethylene (E) 1:1 alternating copolymer. The PCTFE was obtained from 3M Co.(St. Paul, Minnesota) and the CTFE/E co-polymer was acquired from Scientific Polymer Products, Inc. (Ontario, New York). The last group was composed of ester and ether Estane®, and a Solithane® based

cross-linked polyurethane. Ester and ether Estane® were obtained from Prof. J.E.McGrath's polymer synthesis laboratory at Virginia Tech, Blacksburg, Virginia. The characterization data is presented in Table 3. The Solithane® based polyurethane was acquired from Thiokol/Chemical Division (Trenton, New Jersey). Solithane®, a triisocyanate urethane prepolymer of low molecular weight, was polymerized with a polyol (29% by weight), and tri-isopropanol amine (5% by weight) as cross-linking agent. The solvents used were spectrographic grade from Fisher Scientific Co.

TABLE 1

Co-polyesters used for the second group.

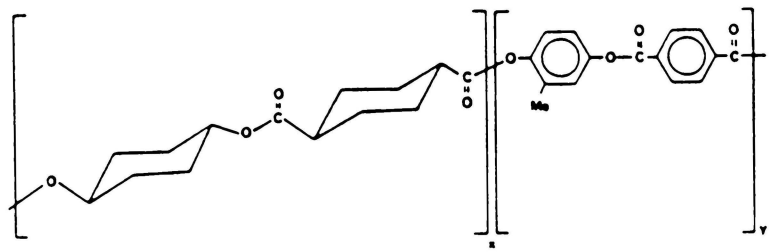

IIIB. *Poly [oxy-trans-1,4-cyclohexylene oxycarbonyl-trans-1,4-cyclohexylene carbonyl-b-oxy (2-methyl-1,4-phenylene) oxy terephthaloyl].*
η_{inh}= 0.85dL/g in 3:1(v/v) CH_2Cl_2/CF_3COOH at 30°C.

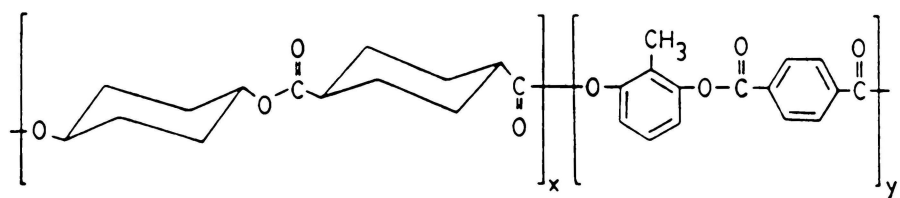

VIIB. *Poly [oxy-trans-1,4-cyclohexylene-oxy carbonyl-trans-1,4-cyclo hexylene carbonyl-b-oxy(2-methyl-1,3-phenylene) oxy terephthaloyl].*
η_{inh}= 0.74dL/g in o-chlorophenol at 30°C.

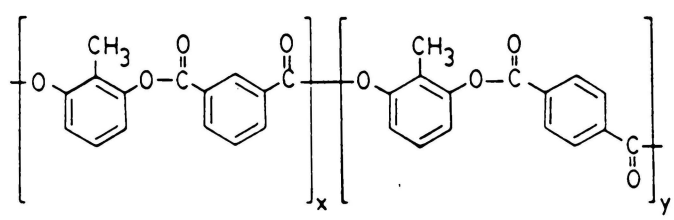

XB. *Poly [oxy(2-methyl-1,3-phenylene) oxy isophthaloyl-b-oxy-(2-methyl-1,3-phenylene) oxy terephthaloyl].*
η_{inh}= 0.60dL/g in 3:1 (v/v) of $CHCl_3/CF_3COOH$ at 30°C.

TABLE 2

Homopolyesters used for the second group.

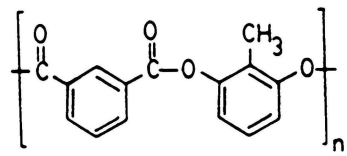

IAR. *Poly [oxy (2-methyl-1,3-phenylene) oxy isophthaloyl].*
η_{inh}= 0.21dL/g in m-cresol at 30°C.

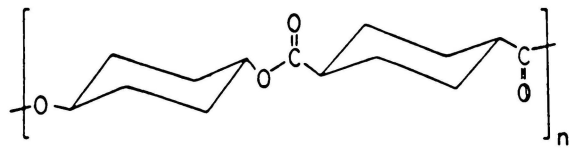

IIIAL. *Poly [oxy-trans-1,4-cyclo hexylene oxy carbonyl-trans-1,4-cyclo hexylene carbonyl].*
η_{inh}= 0.55dL/g in 3:1 (v/v) $CHCl_2/F_3CCOOH$ at 30°C.

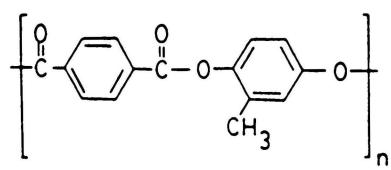

IIIAR. *Poly [oxy (2-methyl-1,4-phenylene) oxy terephthaloyl].*
η_{inh}= 0.58dL/g in 3:1 (v/v) $CHCl_2/F_3CCOOH$ at 30°C.

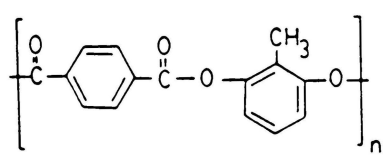

VIIAR. *Poly [oxy (2-methyl-1,3-phenylene) oxy terephthaloyl].*
η_{inh}= 0.52dL/g in o-chlorophenol at 30°C.

TABLE 3

Characterization data for the polyurethanes.

Ester Estane®

31% MDI (hard segments) and 69% TMAD (soft segments).

soft segments 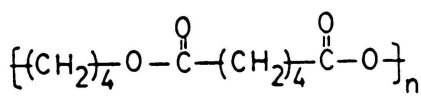 *MW=2000*

hard segments 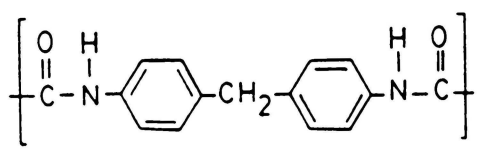

Ether Estane®

35% MDI (hard segments) and 65% PTMO (soft segments).

soft segments 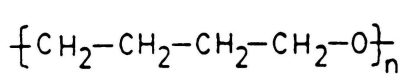 *MW=1000*

hard segments 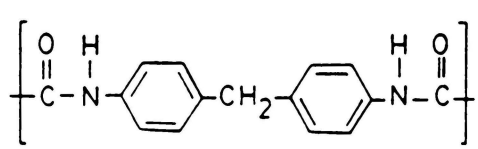

METHODS

The basic methodology was the determination of the chemical composition using XPS in its angle-dependent configuration. As expressed in a preceding section, this method permits the differentiation between the outermost atom layers and the bulk of the polymer. In some cases, characterization with Scanning Electron Microscopy was also performed.

Sample Preparation

Several methods were used for the sample preparation for spectroscopic analysis, namely solution casting, compression molding, and polymerization directly on the probe. In some instances, powders were used for the analysis. Table 4 shows the sample preparation technique used for each system.

Solutions for solution cast films were typically prepared by weighing about 0.5 g. of polymer in a glass vial and dissolving in 20 ml. of solvent to yield a clear solution. Where necessary, filtration of the solution was done. Thin films, about 0.5mm. thick, were cast on carefully cleaned stainless steel strips of dimensions 1"×1/4" suitable to attach directly to the spectrometer probe. Atmospheric evaporation of solvent was allowed for one hour followed by vacuum drying in the introduction chamber of the

TABLE 4

Sample Preparation methods

Polymer	Sample preparation	Solvent
PET	As received	-----
IIIB	Solution cast	Chloroform
VIIB	Solution cast	Chloroform
XB	Solution cast	Chloroform
IAR	Powder as received	-----
IIIAL	Powder as received	-----
IIIAR	Powder as received	-----
VIIAR	Powder as received	-----
PCTFE	Compression-molded	-----
E/CTFE	Compression-molded	-----
Ester Estane®	Solution cast	Tetrahydrofuran
Ether Estane®	Solution cast	Tetrahydrofuran
Solithane® based polyurethane	Polymerization on probe	-----

spectrometer. Samples were analyzed right after vacuum drying to ensure a minimum atmospheric contamination, if any.

Polymerization on clean stainless steel strips was utilized for the cross-linked Solithane® based polyurethane. The reactants were mixed together and the mixture cast on a clean stainless steel strip. Then, the mixture was heated to 80°C. in an oven and let react for 6 hours. Finally, the cross-linked film was allowed to cool down to room temperature. Films 1 mm thick were obtained by this procedure.

Compression molded films were pressed at 240°C. in a hydraulic press between scrupulously clean aluminum foil. The aluminum foil was removed immediately before introduction of the sample into the analysis chamber.

Instrumentation

The x-ray photoelectron spectrometer used in this investigation was a XSAM 800 Model, manufactured by Kratos Ltd., England. This state-of-the-art commercial instrument is equipped with a dual anode x-ray source and a hemispherical electron energy analyzer. Automatic data adquisition and simultaneous data processing is enabled by means of a DEC RT11 computer system interfaced to the spectrometer.

The stainless steel strips with the cast films were attached to the sample holder with the aid of screws. Samples compression molded and samples used as received were mounted using double stick adhesive tape. All the spectra were collected using the Mgk$\alpha_{1,2}$ x-ray source run at 13 kV. and 20 ma. The pressure in the analysis chamber was maintained at about 10^{-9} torr. during data collection. The analyzer was operated in the Fixed Retardation Ratio (FRR) mode. When valence band spectra were collected, core level spectra were obtained previously and subsequently to the valence band spectra to check for possible degradation of the polymers after long exposure to x-ray radiation.

Angle-depth profiling was performed varying the electron take-off angle 0 between the analyzer and the sample surface. This was achieved by rotating the probe rod to the required degree. Electron exit angles of 90°, 30° and 10° were typically used.

A Jeol Model 35C scanning electron microscope at 25 kV. was used.

XPS Data Processing

In this section, the general procedure used to transform the spectroscopic data into useful numbers is discussed.

Equation 3.7 was used to calculate atomic fraction ratios. C1s, O1s, F1s, N1s, and C12p levels were used for the purpose. The configuration of the XSAM 800 instrument is such that the angle between the incident x-rays and the ejected electrons, α, is 54.6°, the "magic angle". Therefore, in Equation 3.7 the differential cross-section, $\partial\sigma_k/\partial\Omega$, is equal to the total cross-section σ_k for all the atomic levels. As the spectrometer was operated in the Fixed Retardation Ratio (FRR) mode, the transmission function, T(E), is just the kinetic energy of the electrons analyzed. The values for the mean free paths[92], cross-sections[84] and kinetic energies used are shown in Table 5. The data presented are averages of at least two determinations. Energy referencing was done with respect to the hydrocarbon component of the C1s spectrum at BE = 285.0 eV. Curve fitting was performed utilizing Gaussian line shapes for the component peaks.

TABLE 5

XPS parameters for the calculation of atomic fraction ratios.

Atomic Level	C1s	O1s	N1s	F1s	C12p
Electron kinetic energy, eV	967	723	852	568	1054
Total cross-section, kilobarns	22.2	63.3	39.3	94.6	52.4
Mean Free path, angstroms	18.2	14.6	16.5	12.2	19.4

Chapter V

RESULTS AND DISCUSSION

This chapter is divided into four sections devoted to poly (ethylene terephthalate), block copolyesters, fluorine containing polymers and polyurethanes, respectively.

POLY (ETHYLENE TEREPHTHALATE)

As mentioned above, poly (ethylene terephthalate) (PET) samples of 22%, 29%, 39% and 51% crystallinity were used for this study. Figure 14 shows the wide scan spectra of PET at normal exit angle. The O1s and C1s photoelectron lines are observed, and no contamination can be distinguished. In Figures 15, 16, and 17 experimental narrow scan spectra of PET of different degrees of crystallinity is presented alongside with spectra from the literature[104]. In all spectra, three component peaks under the C1s spectra and two components under the O1s envelope can be recognized, as shown in the computer curve-fitted peaks. The C1s components are located at binding energies of 285.0 eV. assigned to carbons from the benzene ring, 286.6 eV. corresponding to the singly bonded carbon-to-oxygen, and 289.0 eV. associated to the doubly bonded carbon-to-oxygen group of the carboxylate. The O1s component peaks are located at 532.1 eV. for doubly bonded oxygen-to-carbon and 533.7 eV. for

singly bonded oxygen-to-carbon. The peak positions, as well as the O/C relative atomic ratio (0.37) are in good agreement with data from the literature[104]. However, comparison of the line shapes indicates some differences between the data obtained in this investigation and the data obtained by Dwight et al.[104], specifically on the O1s spectra. The O1s spectra shown in the present study has a doubly bonded oxygen-to-carbon component of higher intensity than the singly bonded oxygen-to-carbon component. Whereas, the spectra collected by Dwight et al. presents a 1:1 ratio between the two O1s component peaks. Nevertheless, the O/C relative atomic ratio (0.37) does not indicate oxydation of the polymer surface.

Further characterization of the specimens was attempted using Scanning Electron Microscopy. The photomicrographs obtained are presented in Figure 18. The presence of a crystalline structure on the surface of the specimen is observed. These crystals, in general, have the form of hexagonal prisms. These structures were observed before in annealed PET samples. Perovic and Sundararajan[105] analyzed this type of crystals and they were found to be cyclic oligomers of low molecular weight, with three repeating units.

It is interesting to observe in Figure 18 the oligomer crystallites grow from almost nucleation to fully developed

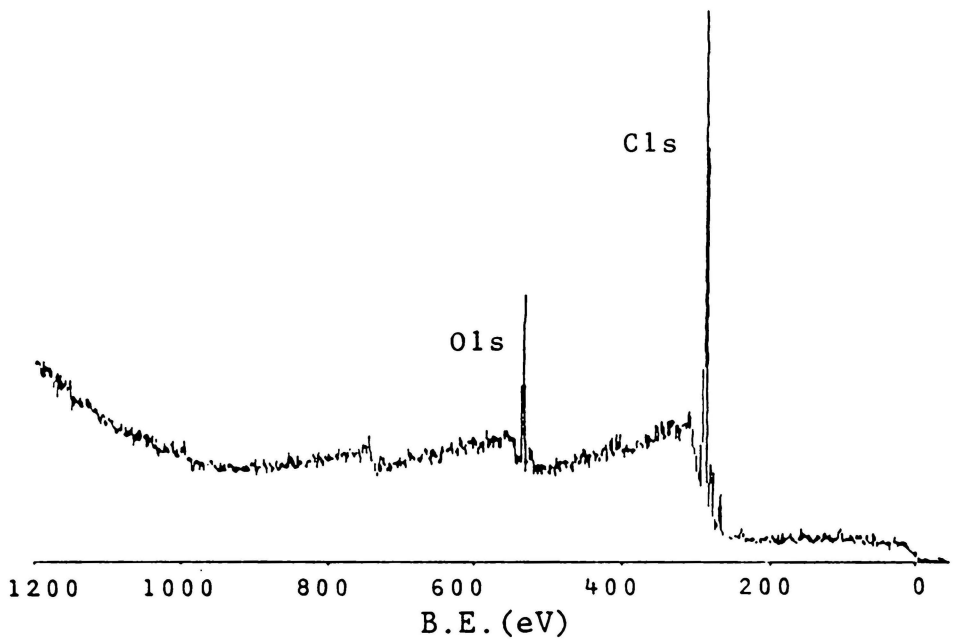

Figure 14: Wide scan XPS spectrum of poly (ethylene Terephthalate).

a) 22%

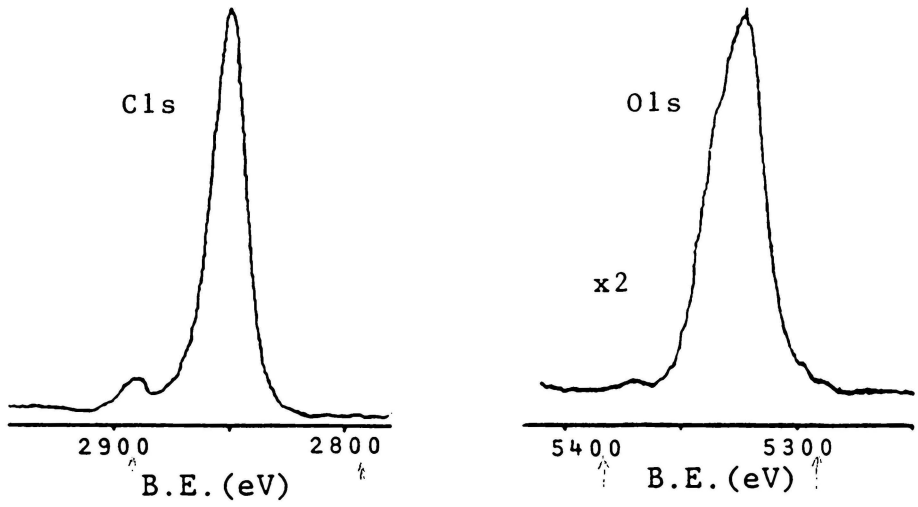

b) 29%

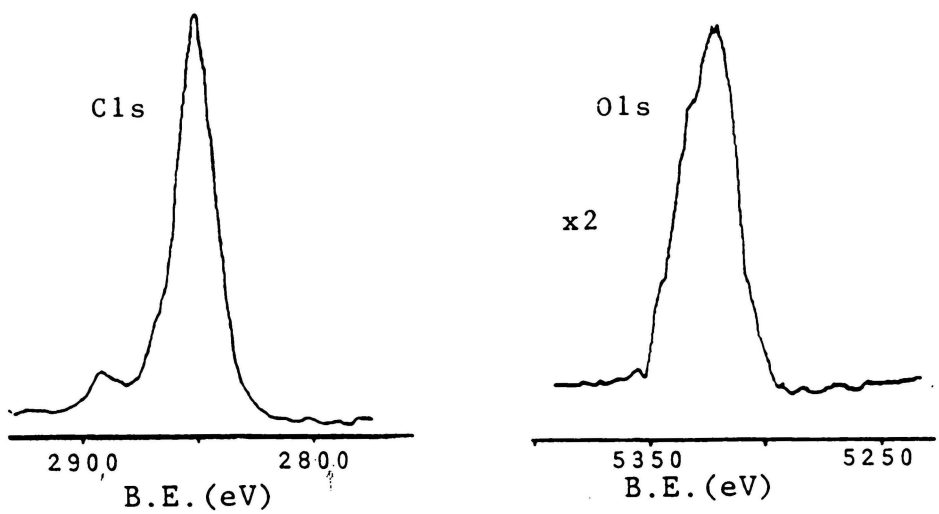

Figure 15: C1s and O1s XPS spectra of PET of a) 22% and b) 29% crystallinity.

a) 39%

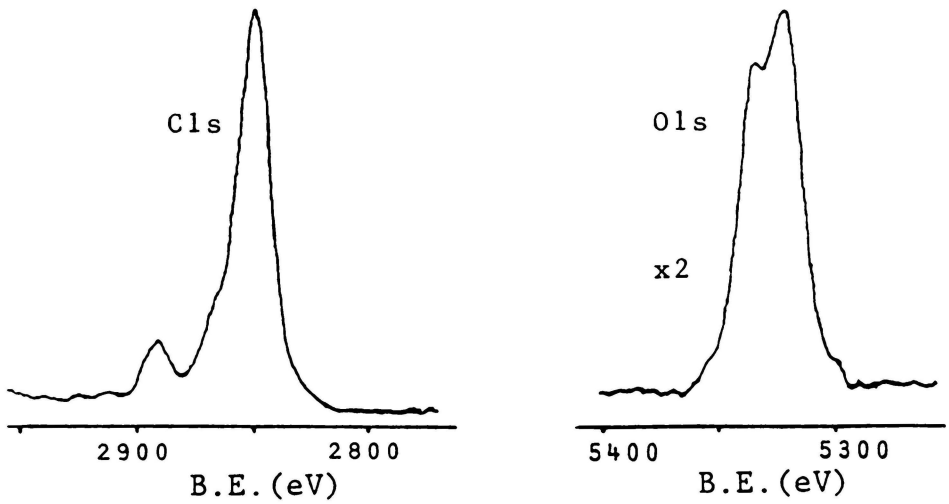

b) Literature

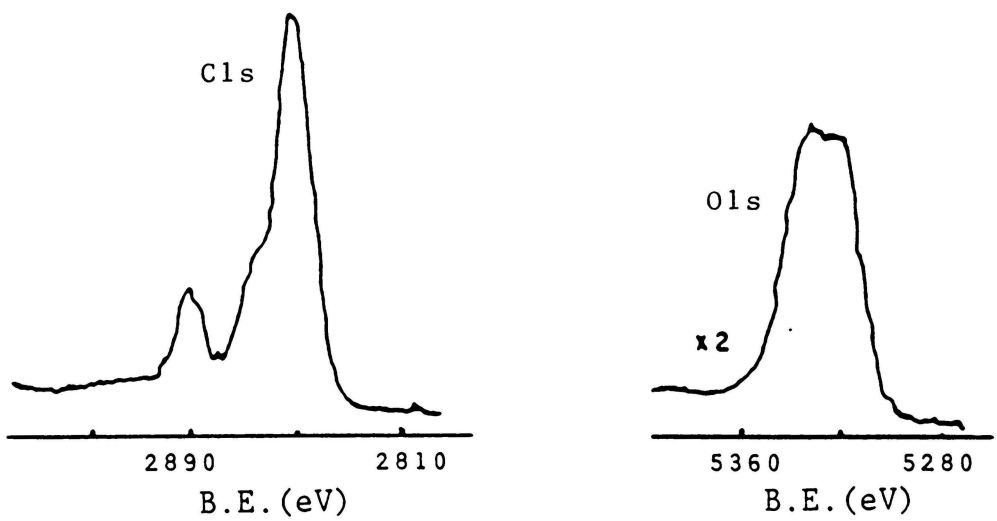

Figure 16: C1s and O1s XPS spectra of PET of a) 39% crystallinity and b) from the literature. [from 104]

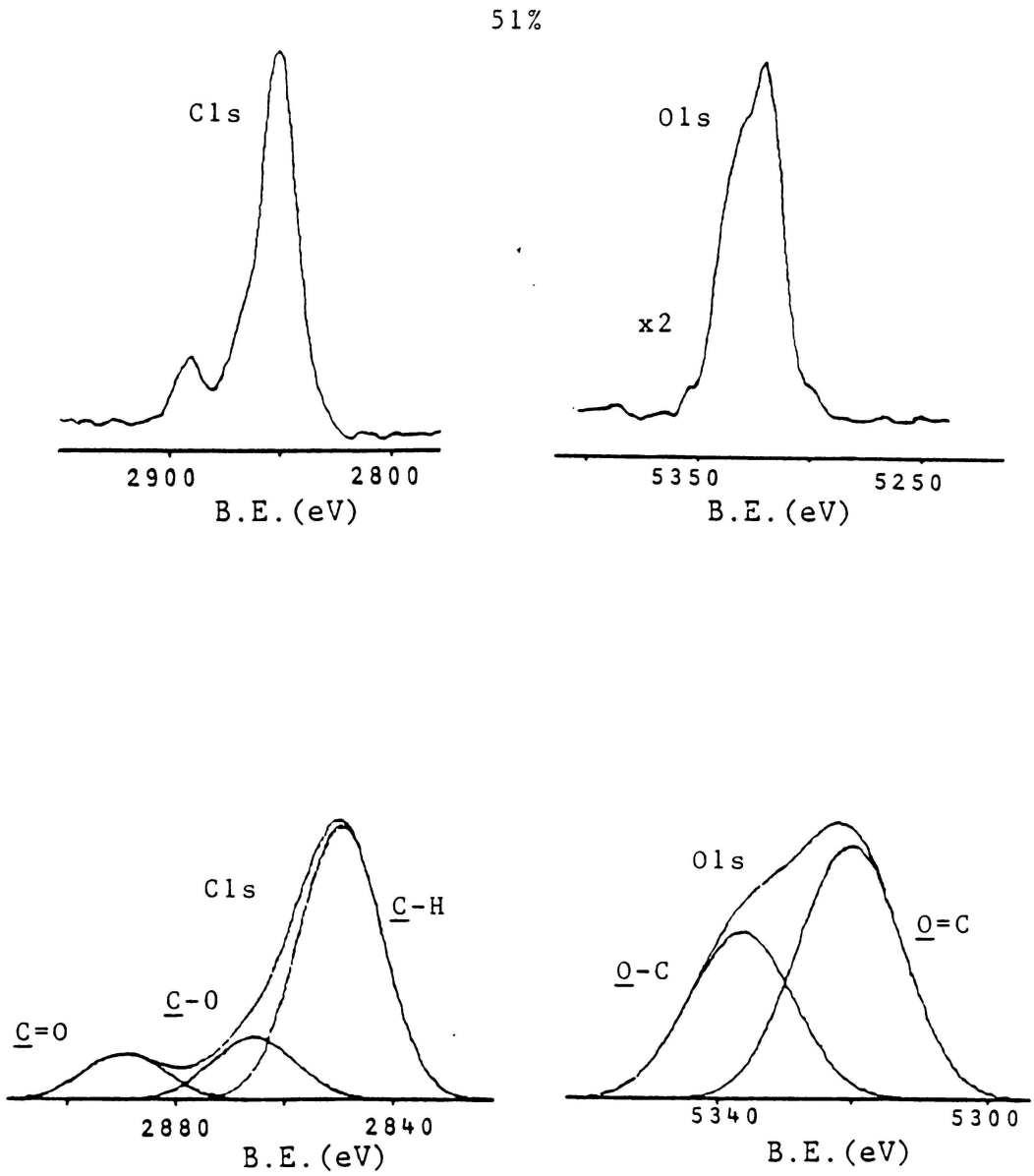

Figure 17: C1s and O1s XPS spectra of PET of 51% crystallinity and representative curve-fitted envelope.

crystals as the crystallinity of the PET samples is increased by annealing. Nucleation takes place at the surface due to the presence of a larger amount of defects as well as different crystalline structure of the cyclic oligomers than the PET matrix. Migration of the cyclic oligomers has to occur so that crystallization can happen. Therefore, diffusion of the cyclic oligomers towards the surface of PET takes place during annealing.

Although these cyclic oligomers were studied by SEM[105], they were not known to alter the XPS spectra of PET. In an attempt to confirm this fact, a chloroform extraction[105] of a PET sample of 51% crystallinity was performed for twelve hours. Figure 19 depicts micrographs and XPS spectra obtained after the chloroform extraction. The hexagonal crystals are completely removed from the surface of the PET sample as shown in Figure 19. However, indentations left by the oligomer crystals are observed. A higher magnification micrograph reveals the different textures of the site where an oligomer crystal was located and the rest of the PET matrix. The XPS spectra of PET after the extraction are very resemblant of those observed in the literature[104], i.e., the singly bonded oxygen-to-carbon and the doubly bonded oxygen-to-carbon components of the O1s spectrum are present in a 1:1 ratio.

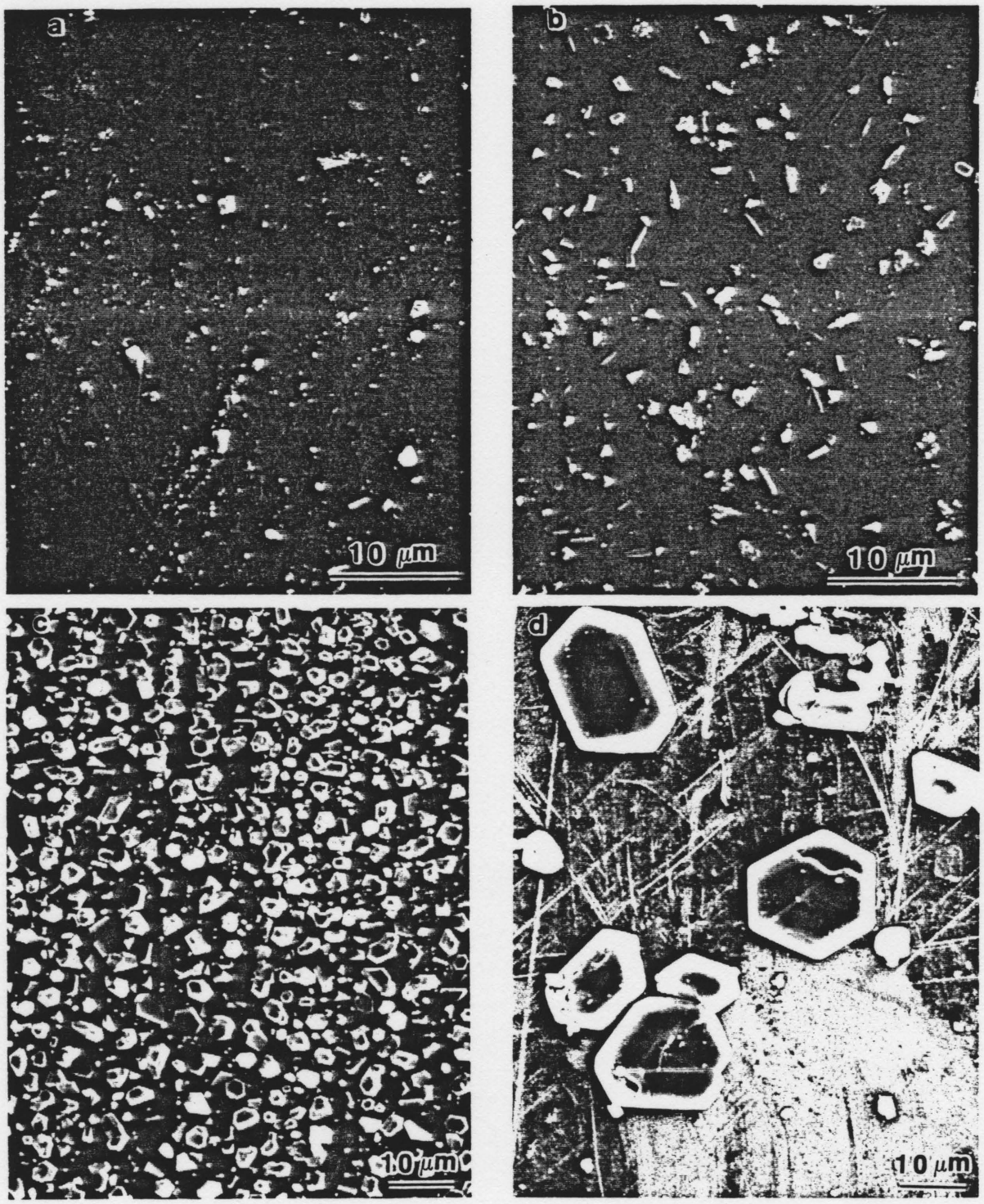

Figure 18: SEM micrographs of a) 22%, b) 29%, c) 39%, and d) 51% crystallinity content.

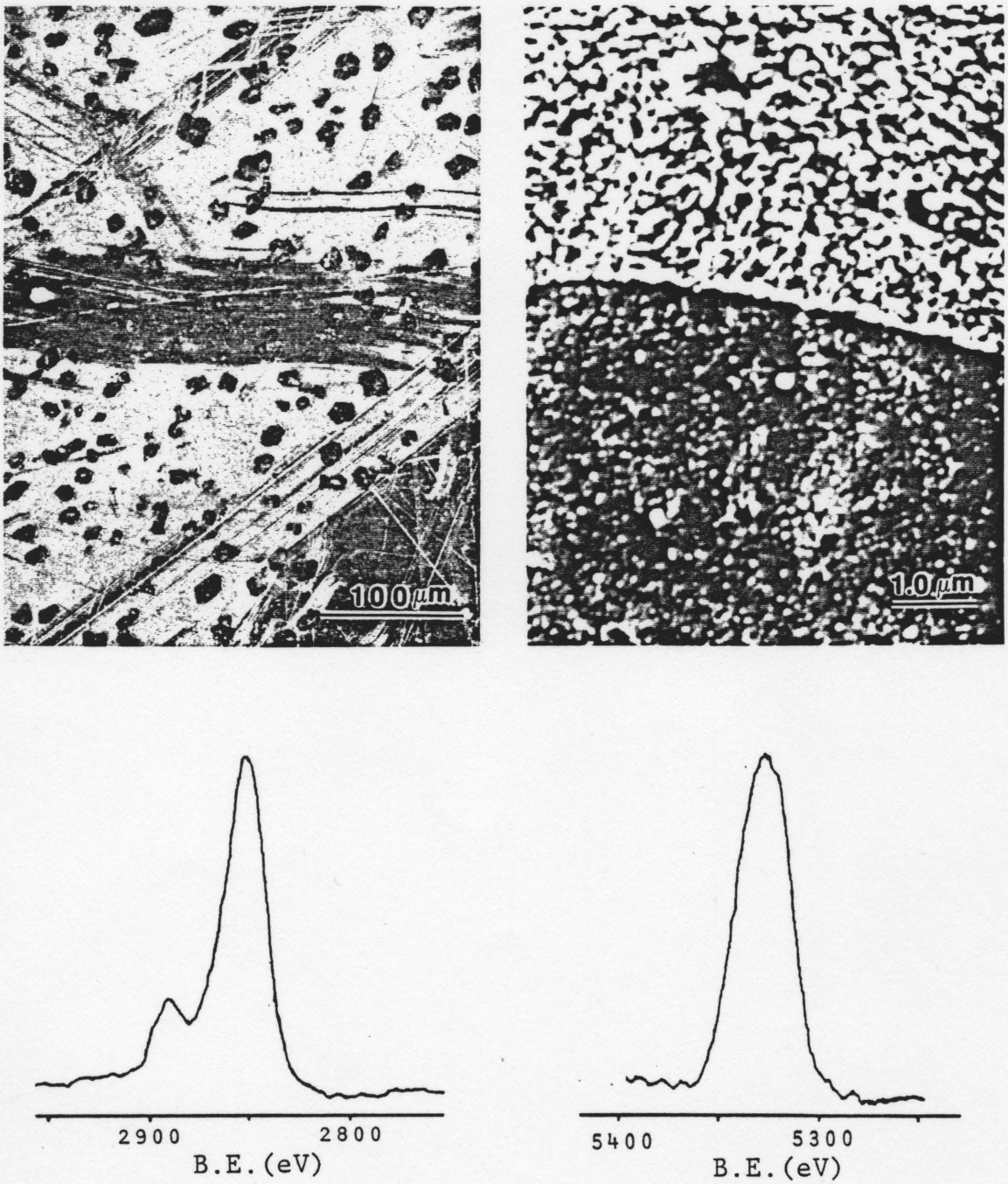

Figure 19: SEM micrographs and C1s and O1s XPS spectra of PET of 51% crystallinity after $CHCl_3$ extraction for 12 hs.

The cyclic oligomers are believed to be composed of three repetitive units[105]. Neither the stoichiometry nor the chemical bonds of the cyclic oligomers are different from those of PET. Therefore, no difference is observed either in the O/C ratio or binding energy shifts of the PET samples that contain the cyclic oligomer at the surface. However, it is clear that the peak profiles corresponding to the O1s levels of PET are affected by the presence of the cyclic oligomer on the surface. Consequently, XPS is capable of detecting the presence of this cyclic oligomer, provided that it is present at the surface.

It is noteworthy to comment on two possible applications of the exudation effect observed. First, the determination of the degree of crystallinity of polymers by including a chemical label that is exudated to the surface when the crystallinity increases. If the exudation is quantitative, the amount of chemical label at the surface after annealing of the sample can be quantified by XPS and related to the degree of crystallinity of the specimen. Second, the extraction of the oligomer crystallites by chloroform leaves behind a very interesting surface topography. Consequently, modification of the surface topography can be achieved by annealing PET that contains cyclic oligomers and extracting, afterwards, with chloroform.

BLOCK COPOLYESTERS AND HOMOPOLYESTERS

In this section, the data corresponding to materials of the second group are presented and discussed.

As shown by the chemical structure of the polymers comprising this group in Tables 1 and 2, there is no difference in the O/C stiochiometric ratios. Therefore, the application of O1s/C1s relative atomic ratios determined by XPS are of no use for the characterization and differentiation of these polymers. However, since the block copolyesters contain, at least, one aromatic block, shake up satellites are present in the spectra. Consequently, this level of information can be used for the characterization. In particular, the ratios defined as

$$a = \frac{\text{C1s envelope area}}{\text{C1s shake up area}}$$

$$b = \frac{\text{O1s envelope area}}{\text{O1s shake up area}}$$

are used for the characterization of the polyesters, in conjunction with line shape analysis.

Since the differences in chemical structure of the blocks of the polyesters are very subtle, it is mandatory to study the homopolyesters with the chemical composition of each block before attempting characterization of the copolymers. Therefore, this section is divided into two

subsections devoted to homopolyesters and copolyesters, respectively.

Homopolyesters

Figures 20, 21 and 22 depict the core level spectra corresponding to IAR and IIIAR, VIIAR and IIIAL, and computer curve-fitted peaks, respectively. Table 6 shows the binding energies of the core level spectra of the homopolymers. The multicomponent character of the C1s spectra is observed. Three components arising from hydrocarbon linkages (C-H) at BE = 285.0 eV., singly bonded carbon-to-oxygen at BE = 286.6 eV., and doubly bonded carbon-to-oxygen at 289.0 eV. are observed. The binding energies of the core levels of the different homopolymers are in agreement within ±0.2 eV., as shown in Table 6. The presence of a shake up satellite at 7.1 eV. from the hydrocarbon component of the C1s peak is observed in the spectra of the aromatic homopolyesters. Given the energy shift, the satellites can be assigned to $\pi \rightarrow \pi^*$ transitions occurring in the aromatic systems. The C1s shake up satellite line shapes are very similar for all the homopolyesters, indicating that these isomers are not distinguishable by means of C1s shake up satellites as seen in other systems.[64,65]

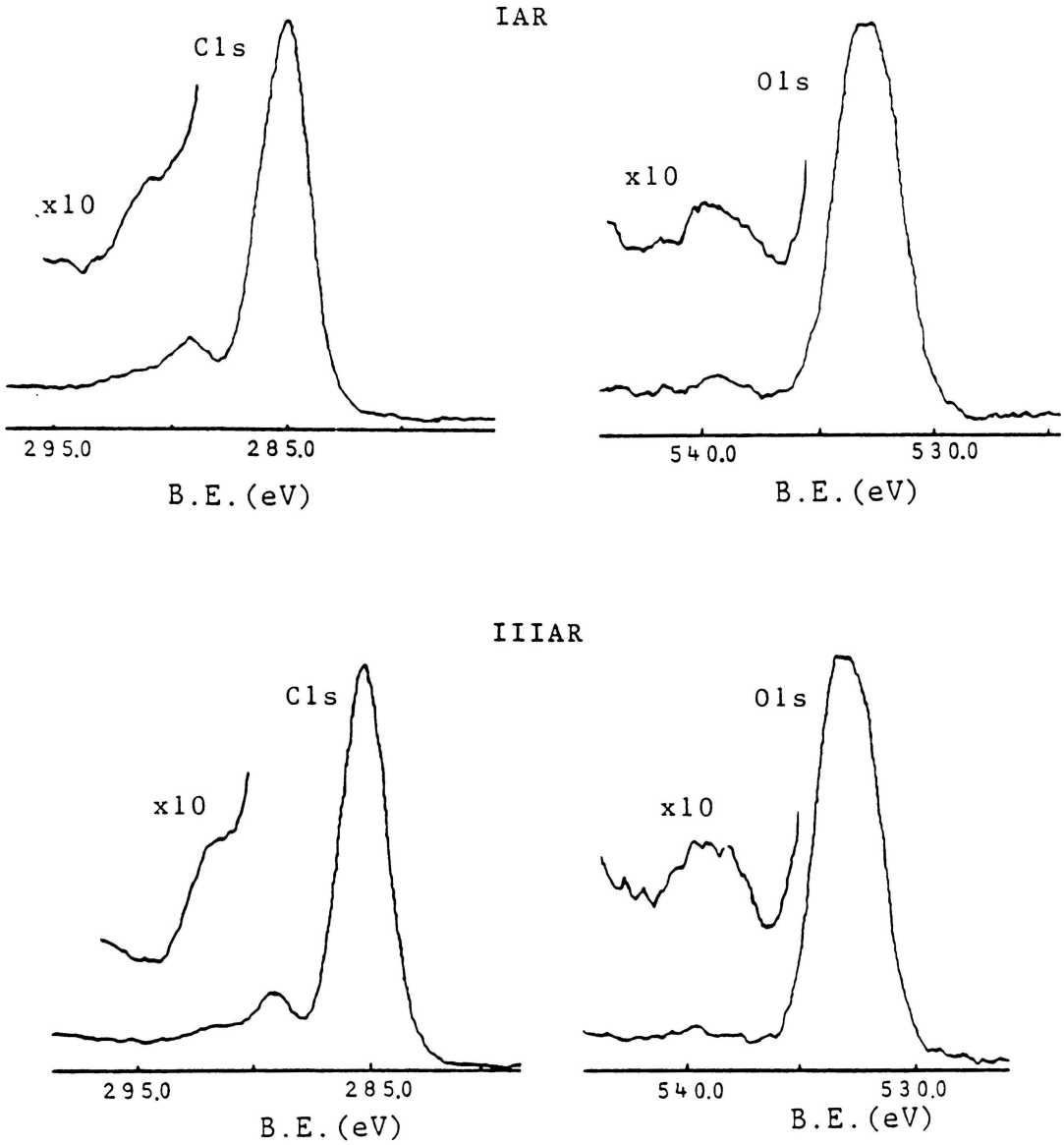

Figure 20: Core level spectra of IAR and IIIAR homopolymers.

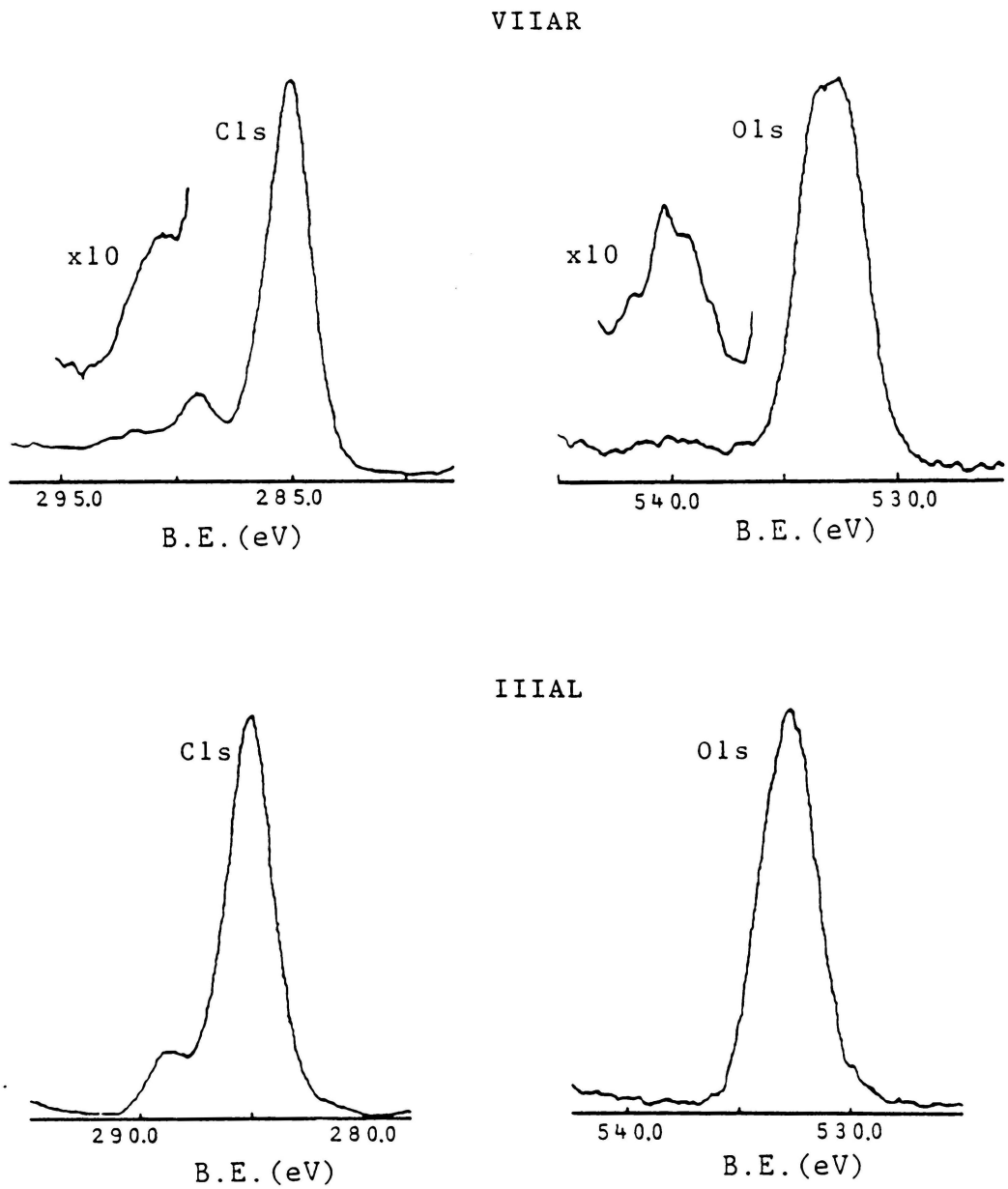

Figure 21: Core level XPS spectra of VIIAR and IIIAL homopolymers.

VIIAR

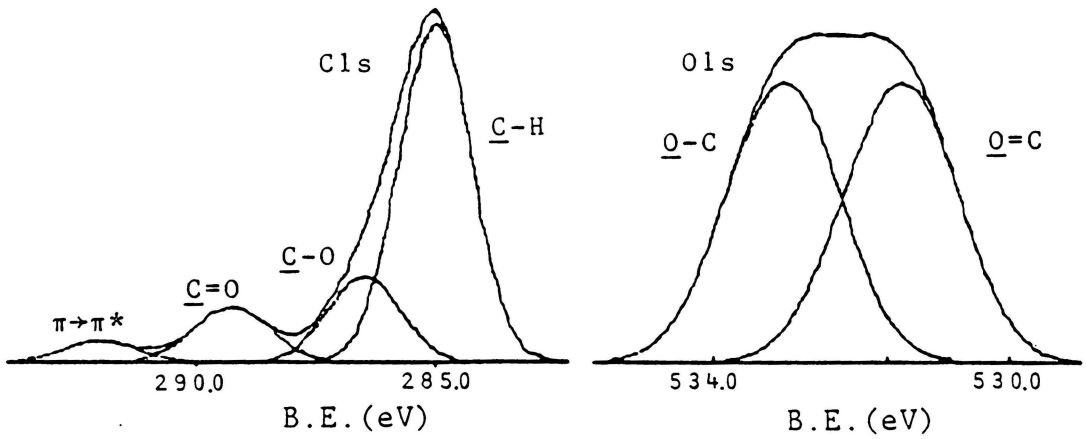

IIIAL

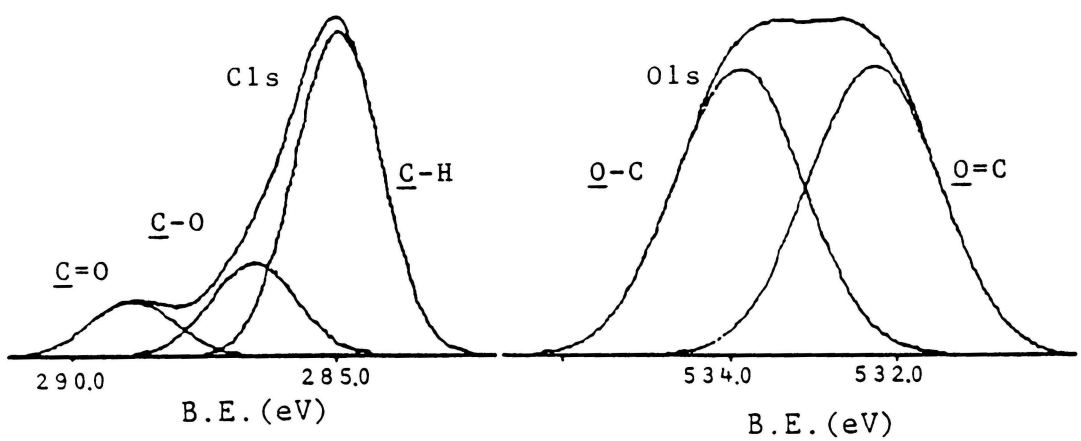

Figure 22: Computer curve-fitted peaks corresponding to a) VIIAR and b) IIIAL.

TABLE 6

Core level binding energies (eV.) for the homopolymers

Homopolymer	C1s*	O1s*	C1s shake-up*	O1s shake-up*
IAR	285.0 286.5 289.1	532.3 533.9	292.1	539.4
IIIAR	285.0 286.5 289.1	532.1 533.7	292.1	539.2
VIIAR	285.0 286.6 289.1	532.2 533.8	292.1	539.3
IIIAL	285.0 286.6 288.9	532.0 533.5	-----	-----

* $\Delta E = \pm 0.2$ eV.

The O1s spectra of the homopolyesters present two component peaks that correspond to oxygen doubly bonded to carbon at BE = 532.1 eV. and to oxygen singly bonded to carbon at BE = 533.7 eV. The O1s spectra pertaining the aromatic polyesters show a shake up satellite at approximately 7.1 eV. from the doubly bonded oxygen-to-carbon component. The energy of the transition is the same of the $\pi \rightarrow \pi^*$ transitions observed in the C1s spectra and the shake up satellites are not observed in the saturated homopolymer IIIAL. Therefore, the O1s shake up satellites suggest some degree of conjugation between the benzene rings and the carboxylate functionalities bonded to the aromatic groups. In particular, the conjugation should occur between the benzene ring and the carbonylic moiety of the carboxylate group, i.e. a delocalization of the π electrons of these two systems. Although of similar origin, the satellite line shapes are characteristic for the three aromatic polyesters as shown in Figure 20 and 21. The different shake up line profiles observed for IIIAR and VIIAR can be attributed to the phenylene groups linked to the terephthaloyl moiety of the polymers,since the chemical structures of IIIAR and VIIAR only differ by the presence of 2-methyl-1,4-phenylene in IIIAR as opposed to 2-methyl-1,3-phenylene group in VIIAR (Table 2). In a similar fashion, the difference in the shake up line shape

of IAR and VIIAR can be attributed to the *meta* position of the carboxilate groups in IAR as opposed to *para* location in VIIAR.

Further information can be obtained if the C1s/C1$^{S}_{S}$ and O1s/O1$^{S}_{S}$ ratios are considered as defined above. Table 7 shows these data for the homopolymers. The three aromatic homopolymers have very similar C1s/C1$^{S}_{S}$ values. However, the O1s/O1$^{S}_{S}$ ratios are strongly different. These results can be interpreted considering the O1s/O1$^{S}_{S}$ ratio as a measurement of the degree of conjugation of the carbonyl and phenylene groups,i.e. the higher the value of the O1s/O1$^{S}_{S}$ ratio, the lower the extent of conjugation. Consequently, the data in Table 7 indicate that VIIAR presents the highest degree of conjugation followed by IIIAR and IAR. In IAR the carboxylate groups are located at *meta* position to each other; thus, IAR has the lowest degree of conjugation and highest O1s/O1$^{S}_{S}$ ratio. On the other hand, the O1s/O1$^{S}_{S}$ values of IIIAR and VIIAR are much lower due to the *para* location of their carboxylate functionalities on the aromatic rings which favors the electron delocalization on these systems. The slight difference on the O1s/O1$^{S}_{S}$ ratios of IIIAR and VIIAR can be explained in terms of the steric hindrance of the methyl group linked to the phenylene moiety of the polymers. In VIIAR, the phenylene group bonded in a 1,3 position can not rotate. Therefore, the bulky methyl

group does not disturb the conjugation on the terephthaloyl group in great extent. In IIIAR, the phenylene group bonded in a 1,4 position can freely rotate as indicated by the following structure:

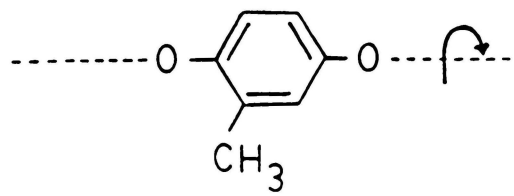

Consequently, the methyl group can lower the degree of conjugation of the terephthaloyl and carboxylate groups giving the slightly higher O1s/O1$_s^s$ value of IIIAR.

As discussed in Chapter II, the valence energy levels can provide interesting information concerning the atomic orbitals involved in the chemical bonds. However, the similarity of the chemical structures of the polymers used in this study makes it difficult to extract much information from these levels of XPS spectra. Nevertheless, Figure 23 presents the valence energy level XPS spectra of the homopolyesters. In all cases, the O2s level located at BE = 27.0 eV. is the best resolved band. Based on the valence band spectra of polystyrene[69] and cyclohexane[106], the rest of the bands can be assigned as follows:

- Bands located at 18 eV. and 14 eV. can correspond to C2s bands, with the 18 eV. band concerning C-C bonding

TABLE 7

C1s area/$C1_s^s$ area and O1s/$O1_s^s$ area ratios for the homopolymers

Homopolymer	C1s/$C1_s^{s*}$	O1s/$O1_s^{s*}$
IAR	7.1	160
IIIAR	7.5	37
VIIAR	7.1	23

* The estimated error is less than ±10%.

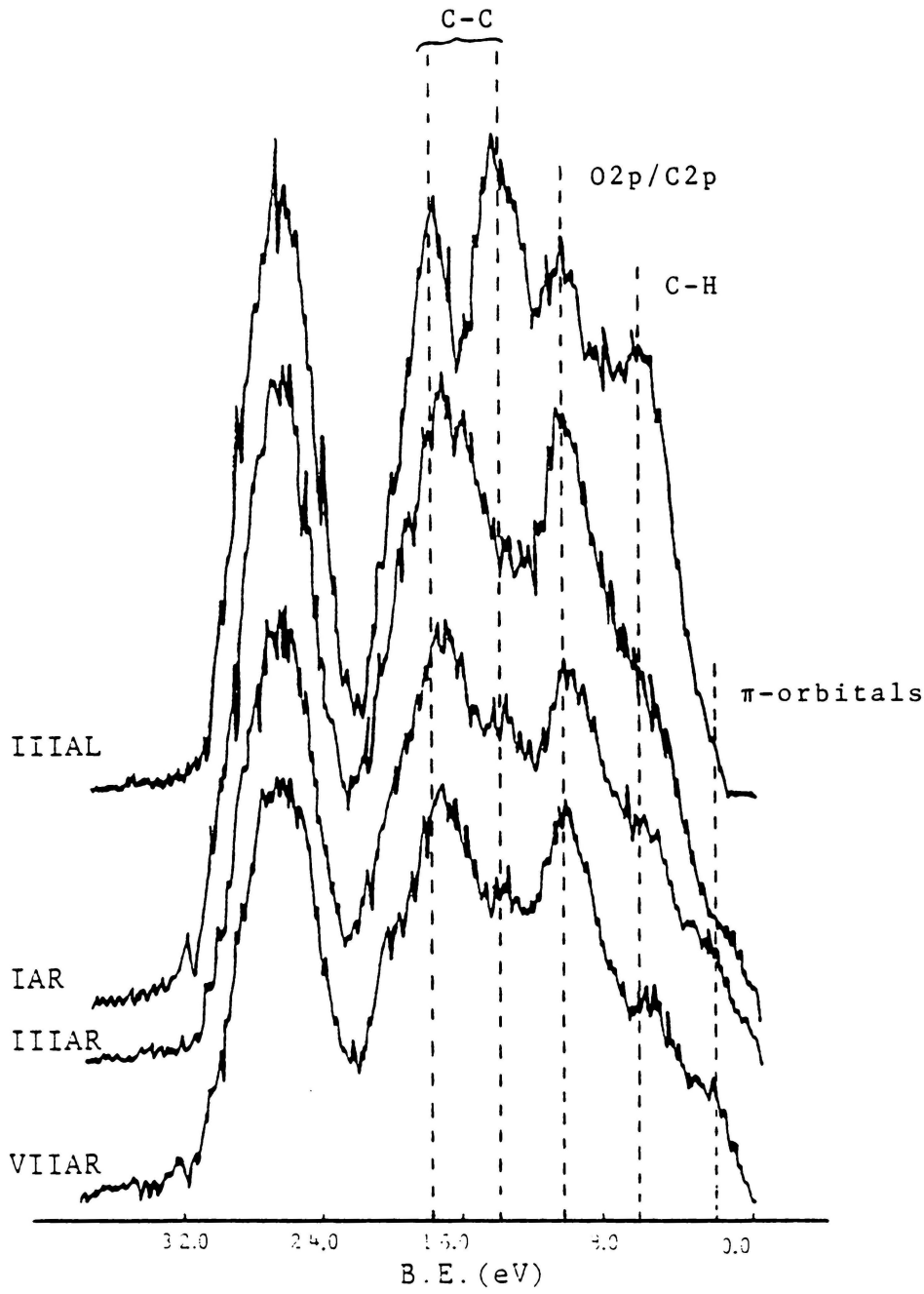

Figure 23: Valence energy level spectra of the homopolyesters.

orbitals and the 14 eV. band corresponding to the antibonding combination of C2s atomic orbitals.

- Bands present at 10 eV. and 6.8 eV. can be attributed to C2p and O2p orbital contributions. The Band at 10 eV is given by the combination of O2p and C2p orbitals in C-O bonds. Whereas, the 6.8 eV. band is produced by molecular orbitals corresponding to the O2p π non-bonding lone-pair superimposed to C-H bonding molecular orbital bands.
- The aromatic homopolyesters present a series of bands at about 3.6 eV. that correspond to the π orbitals concerned with the shake up trnasitions. These bands are not present in the aliphatic polyester IIIAL.

It is interesting to note the better band resolution and narrower bands that are observed in the valence energy levels of the saturated homopolymer IIIAL. It is believed that this is due to the absence of conjugation of π systems in the saturated homopolymer.

Copolyesters

After having discussed the characterization of the homopolyesters, the analysis of the copolyesters is treated in this section.

Figure 24 depicts the core level spectra of IIIB, VIIB and XB copolyesters, with representative curve-fitted

spectra. Table 8 presents the core level binding energies found for this polymers. The C1s level spectra show components at BE = 285.0 eV. (C-H), BE = 286.5 eV. (C-O) and BE = 289.1 eV. (C=O). Shake up satellites are observed located at 7.1 eV. from the hydrocarbon component of the C1s spectra that arise from $\pi \rightarrow \pi^*$ transitions occurring on the aromatic blocks. The C1s line shape is similar for the three polymers as shown in Figure 24. However, the C1s shake up satellite of XB is slightly different from those corresponding to IIIB and VIIB, being these last ones similar to each other. This may be expected since XB is an all aromatic copolymer and VIIB and IIIB have a saturated block in their structure.

The O1s level spectra present two components at BE = 432.1 eV. (O=C) and BE = 533.7 eV. (O-C). Similar to the homopolymers, a shake up satellite located at 7.1 eV. from the O=C component of the O1s spectra is observed. The O1s shake up satellite is attributed to $\pi \rightarrow \pi^*$ transitions occurring in the carbonyl group of the carboxylate functionality, suggesting some degree of conjugation between these groups and the aromatic rings. The shake up satellite line shapes are characteristic for each block copolymer, indicating their "finger-print" character. The O1s shake up line shapes for VIIB and IIIB do not resemble those of the homopolymers VIIAR and IIIAR, respectively. However, the

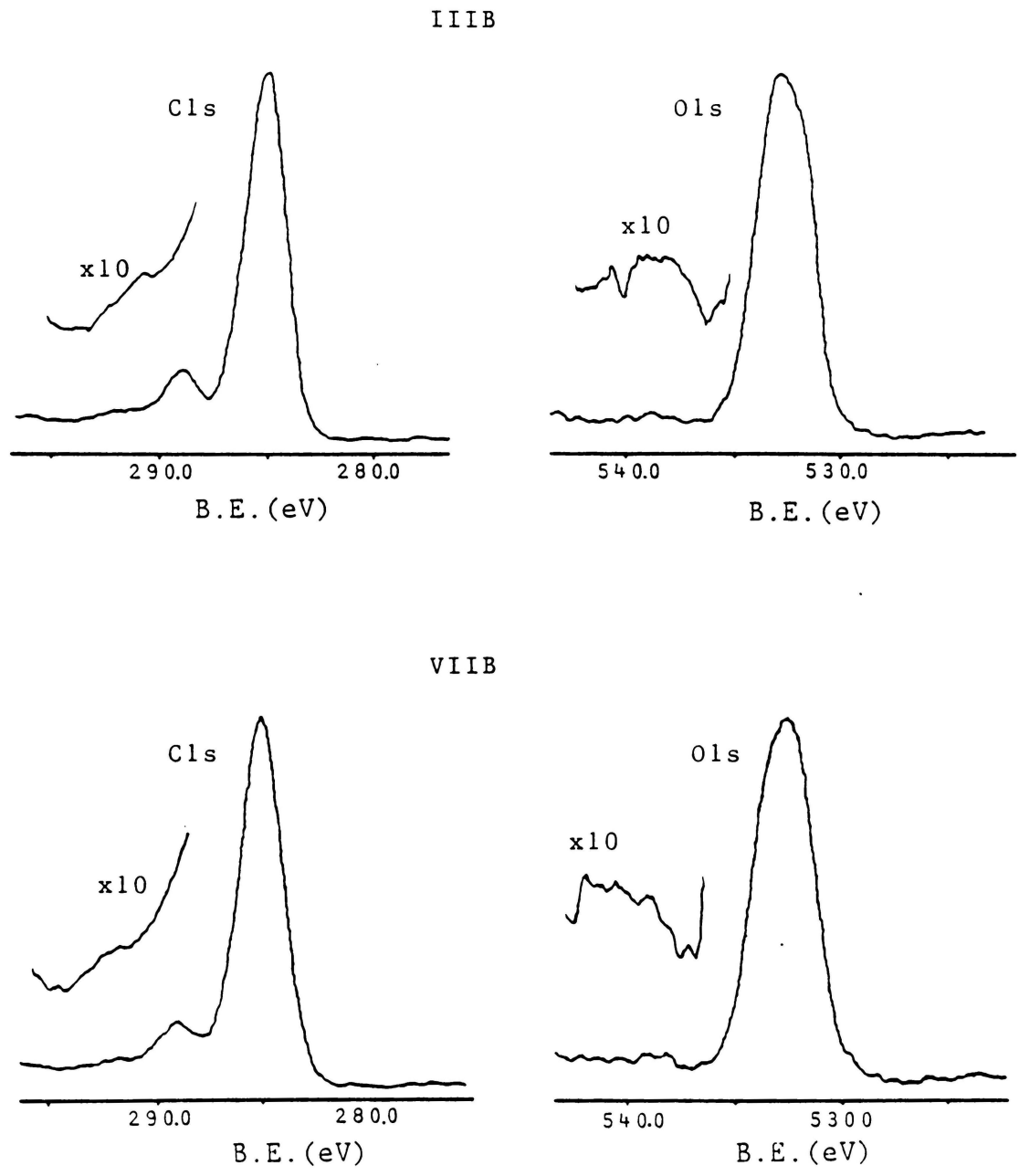

Figure 24: Core energy level spectra of the copolyesters: a) IIIB, b) VIIB, c) XB and d) curve-fitted spectra.

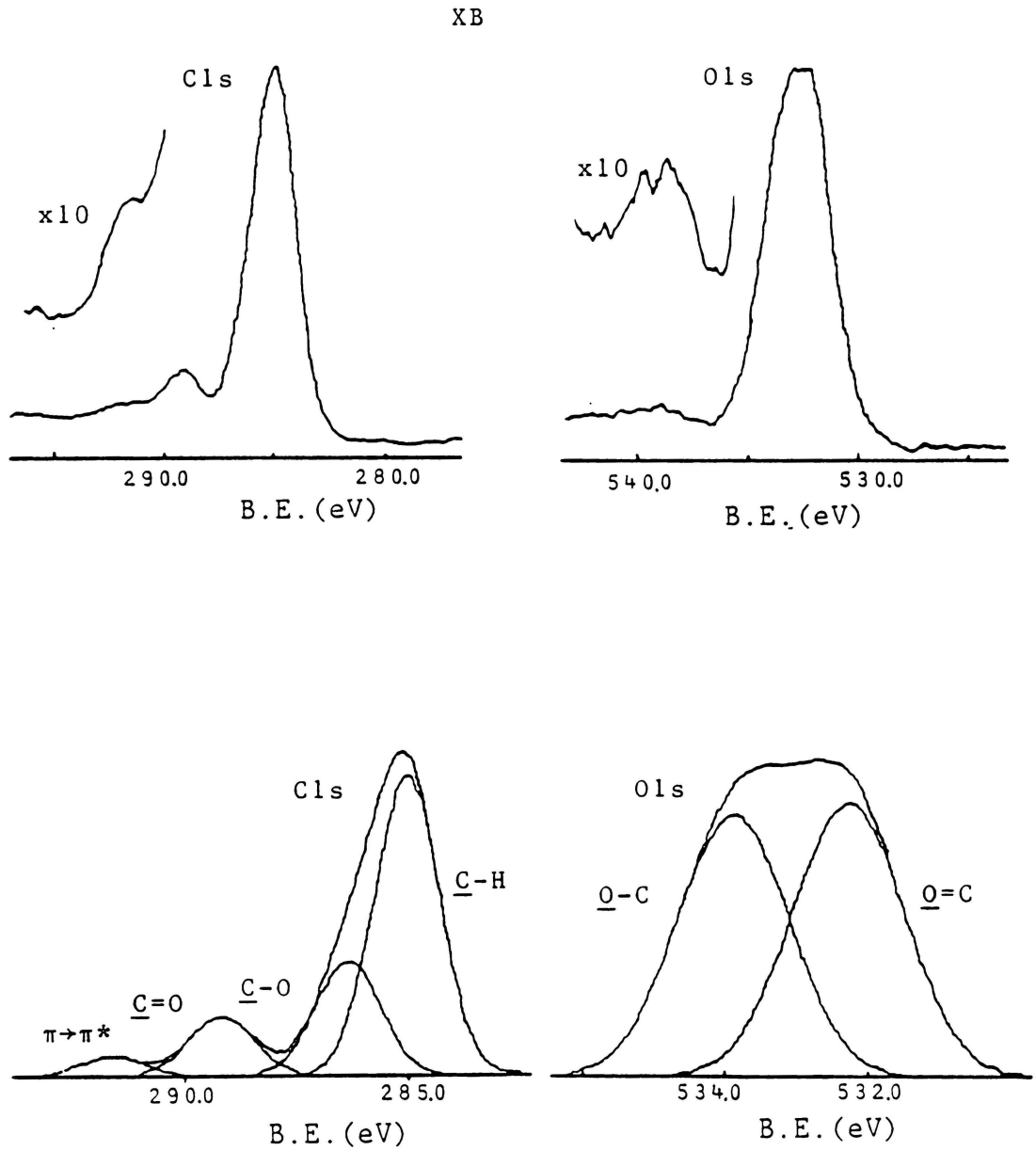

Figure 24: Continued

TABLE 8

Core level binding energies (eV.) for the copolyesters

polymer	C1s*	O1s*	C1s shake-up*	O1s shake-up*
IIIB	285.0 286.5 289.0	532.1 533.7	292.1	539.2
VIIB	285.0 286.5 289.1	532.1 533.7	292.2	539.3
XB	285.0 286.6 289.2	532.2 533.8	292.1	539.2

* $\Delta E = \pm 0.2$ eV.

aromatic blocks of VIIB and IIIB are the same chemical structure of VIIIAR and IIIAR, correspondingly. Therefore, the presence of the saturated blocks linked to the aromatic groups may have affected the satellite line shape. As expected, since XB has two aromatic blocks, no resemblance between the O1s shake up satellite of XB and, VIIAR and IAR is found.

Figure 25 shows the valence energy level spectra corresponding to the copolyesters. The resemblance of these spectra to those of the homopolymers is noticeable. However, the "fingerprint" character of the valence energy level spectra can be observed. Based on the assignments performed on the homopolymers' valence band spectra, the following bands are observed on the copolyesters' spectra:

- O2s level band located at 27.0 eV.
- C2s level bands at 17.8 eV. and 13.7 eV.
- Bands corresponding to O2p and C2p orbital combination in C-O bonds located at 10.0 eV.
- Molecular orbitals corresponding to the O2p π non-bonding lone-pair superimposed to C-H bonding molecular orbital bands at 5.6 eV.
- Bands at 3.3 eV. corresponding to π orbitals concerned with the shake up transitions.

The better resolution of the C2s band at 13.7 eV. is noticed in the spectra of the polymers containing a saturated block,

IIIB and VIIB. As expected, copolymer XB presents a higher intensity band at 3.6 eV. than IIIB and VIIB. Since XB is composed of two aromatic blocks, the probability for $\pi \rightarrow \pi^*$ transitions to occur is higher than in IIIB and VIIB. Therefore, this band, concerned with the π orbitals involved with shake up transitions has higher intensity in the spectra corresponding to XB.

As expressed in Chapter II, enhancement of the signal intensity of species present at the surface of specimens can be achieved by means of the angle-dependent XPS configuration. Table 9 presents the angle-dependent XPS data corresponding to the three copolyesters in terms of $C1s/C1_s^s$ and $O1s/O1_s^s$ ratios. IIIB shows an increase of the $C1s/C1_s^s$ and $O1s/O1_s^s$ ratios as the electron exit angle decreases. This indicates that the intensity of the shake up satellites decreases as the surface of the polymer is approached. Since only the aromatic block of IIIB can present shake up satellites, the results imply that the aromatic block (IIIAR) is preferentially segregated towards the bulk of the polymer. In a similar fashion, VIIB also shows an increase in the $C1s/C1_s^s$ and $O1s/O1_s^s$ ratios as the electron exit angle is decreased. However, as shown in Table 9, the change in the ratios in VIIB is stronger than in IIIB. Therefore, the segregation of the saturated block (IIIAL) towards the surface seems to take a greater extent

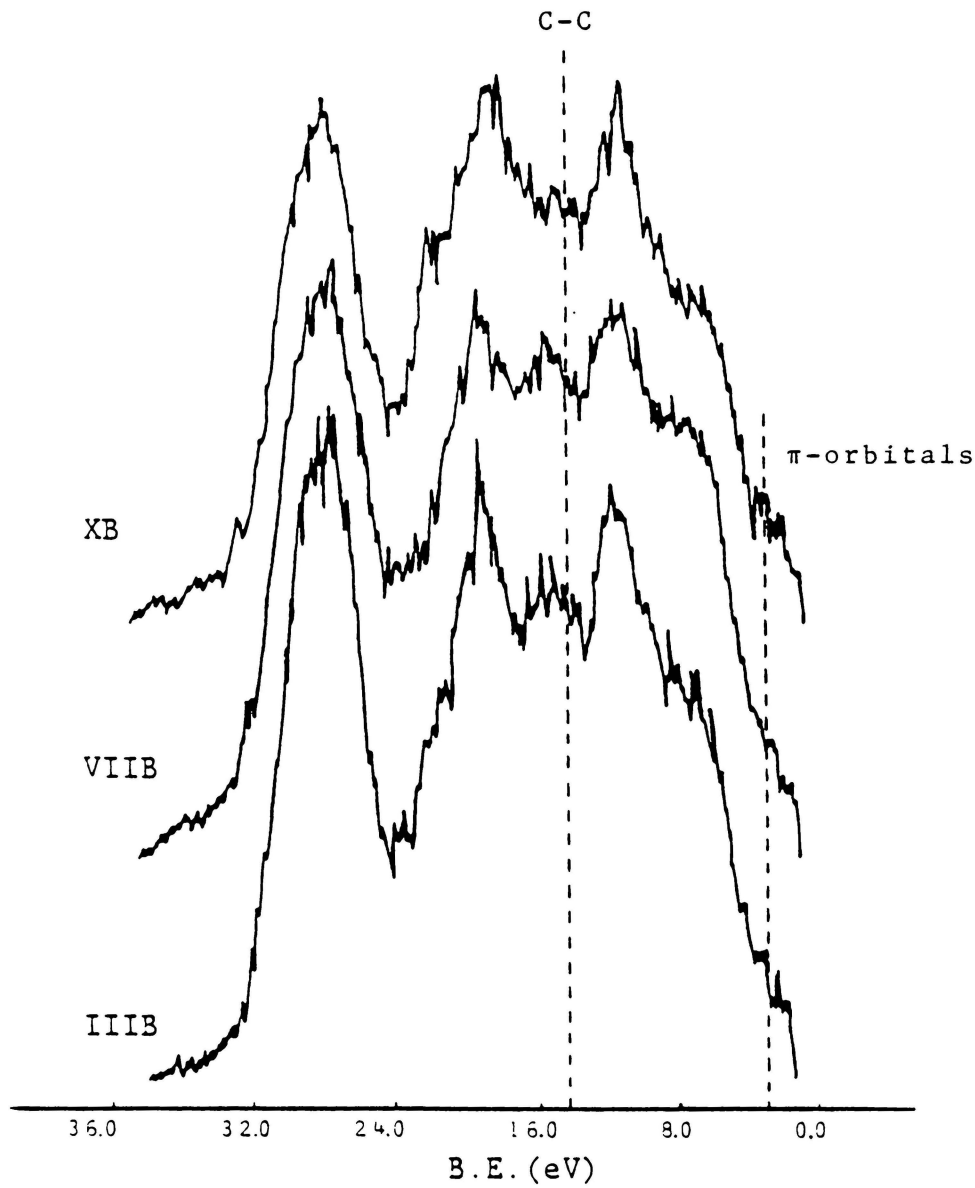

Figure 25: Valence energy level spectra of the copolyesters.

in VIIB than in IIIB. XB has the C1s/$C1_s^s$ ratio approximately constant as the electron exit angle is decreased, consistent with an all aromatic copolymer. However, the O1s/$O1_s^s$ ratio decreases strongly as the electron exit angle decreases. A decrease in the oxygen ratio indicates an increase in the extent of conjugation between the π orbitals of the C=O groups and aromatic rings. The blocks that comprise XB have the chemical structure of IAR and VIIAR and the characterization data of IAR and VIIAR (Table 7) suggested a greater extent of conjugation between the π orbitals of C=O and aromatic groups in VIIAR. Therefore, the decrease of the O1s/$O1_s^s$ ratio of XB suggests the segregation of the block with the chemical structure of VIIAR towards the surface of the polymeric film.

Confirmation of the results cbtained from the angle-dependent XPS spectra of the copolymers may be tested studying blends of the homopolymers, as well as blends of the homopolymers with block copolymers.

TABLE 9

Angle-dependent XPS data for the copolyesters.

polymer	Exit Angle	$C1s/C1s_s$*	$O1s/O1s_s$*
IIIB	10°	12	84
	30°	12	53
	90°	10	54
VIIB	10°	14	208
	30°	14	230
	90°	10	39
XB	10°	11	42
	30°	10	117
	90°	10	278

* The estimated error is less than ±10%.

FLUORINE CONTAINING POLYMERS

The data analyzed in the preceding sections dealt with characterization of homopolymers and the surface segregation in block copolymers. In this section, an alternating copolymer is analyzed. The surface composition of poly (chloro trifluoro ethylene) (PCTFE) is compared with that of an 1:1 alternating copolymer of PCTFE/Ethylene (E).

Figure 26 shows a typical wide scan for a CTFE/E copolymer with labeled peaks. Figure 27 depicts the core level spectra of PCTFE and CTFE/E, as well as the corresponding curve-fitted peaks. Table 10 presents the binding energies measured for these polymers. The C1s spectra of both polymers show multicomponent characteristics. However, the peak line profiles are quite different. Computer curve-fitting of the C1s spectrum of PCTFE brings out two component peaks at BE = 290.4 eV. assigned to CFCL group, and at BE = 291.8 eV. attributed to CF_2 units. As opposed to PCTFE, the C1s spectrum of the copolymer CTFE/E presents four components. The CFCL and CF_2 components are located at BE =290.3 eV. and BE = 291.6 eV., respectively. A C-H component is also observed at BE = 286.5 eV., whereas, carbonaceous contamination is observed at BE = 285.0 eV. The binding energy shift (1.5 eV.) of the C-H component with respect to BE = 285.0 eV. is due to secondary effects produced by the CTFE units adjacent to E units.

This energy shift is in very good agreement with the study done by D.T.Clark[107] on the effect of secondary substituents on the binding energy of a chemical species. If a block copolymer of E/CTFE was to be studied, it can be anticipated that the C1s spectrum would present two components. One component would correspond to CH_2 units adjacent to CF_2 at BE = 286.5 eV., and the other would represent CH_2 groups of the ethylene blocks that are separated from CF_2 units at BE = 285.0 eV. The F1s spectrum is a narrow peak for both polymers. Although only one peak at BE = 689.0 eV. is observed, two components should be present under this envelope corresponding to F-C-F and F-C-Cl groups. However, as expressed by Clark[107], the energy separation of these two components is in the edge of resolution of the energy scale. Therefore, only one component is observed. The Cl2p spectrum is similar for both polymers. It shows two very well resolved components arising from spin-orbit splitting. The component at lower binding energy (200.5 eV.) corresponds to $2p_{3/2}$, whereas that at BE = 202.1 eV. represents the $2p_{1/2}$ spin-orbit.

Figure 28 depicts the valence energy level spectra for PCTFE and CTFE/E polymers. The spectra are dominated by the presence of the F2s photoelectron line at BE = 33.7 eV. Based on the valence energy level spectra of fluoropolymers[67] and of poly (vinyl chloride)[69], the following assignments may be performed:

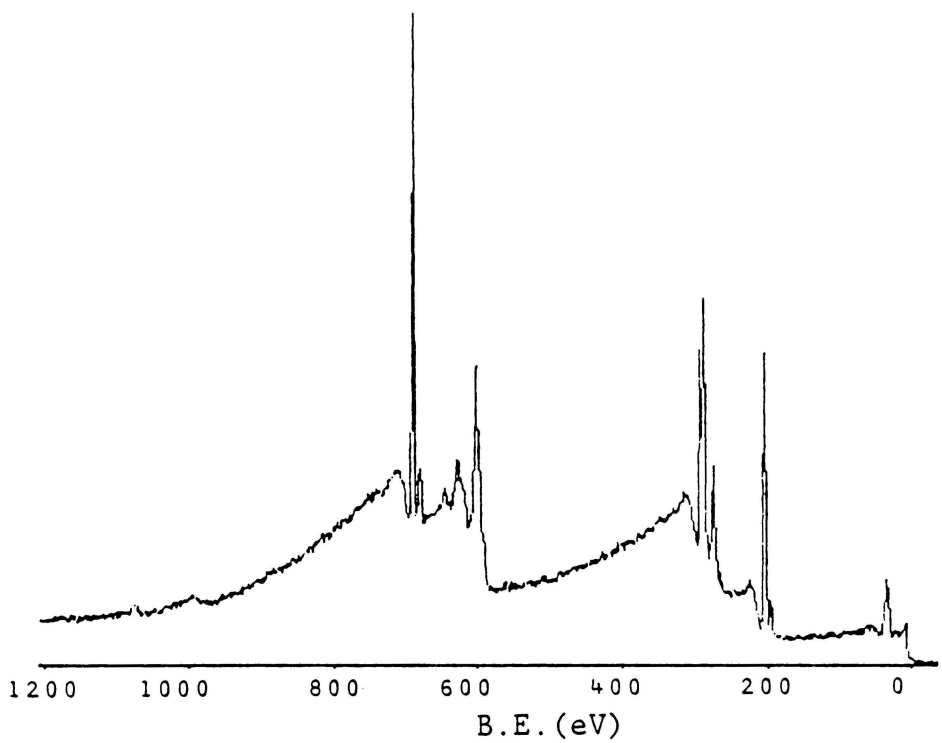

Figure 26: Typical wide scan for a CTFE/E copolymer.

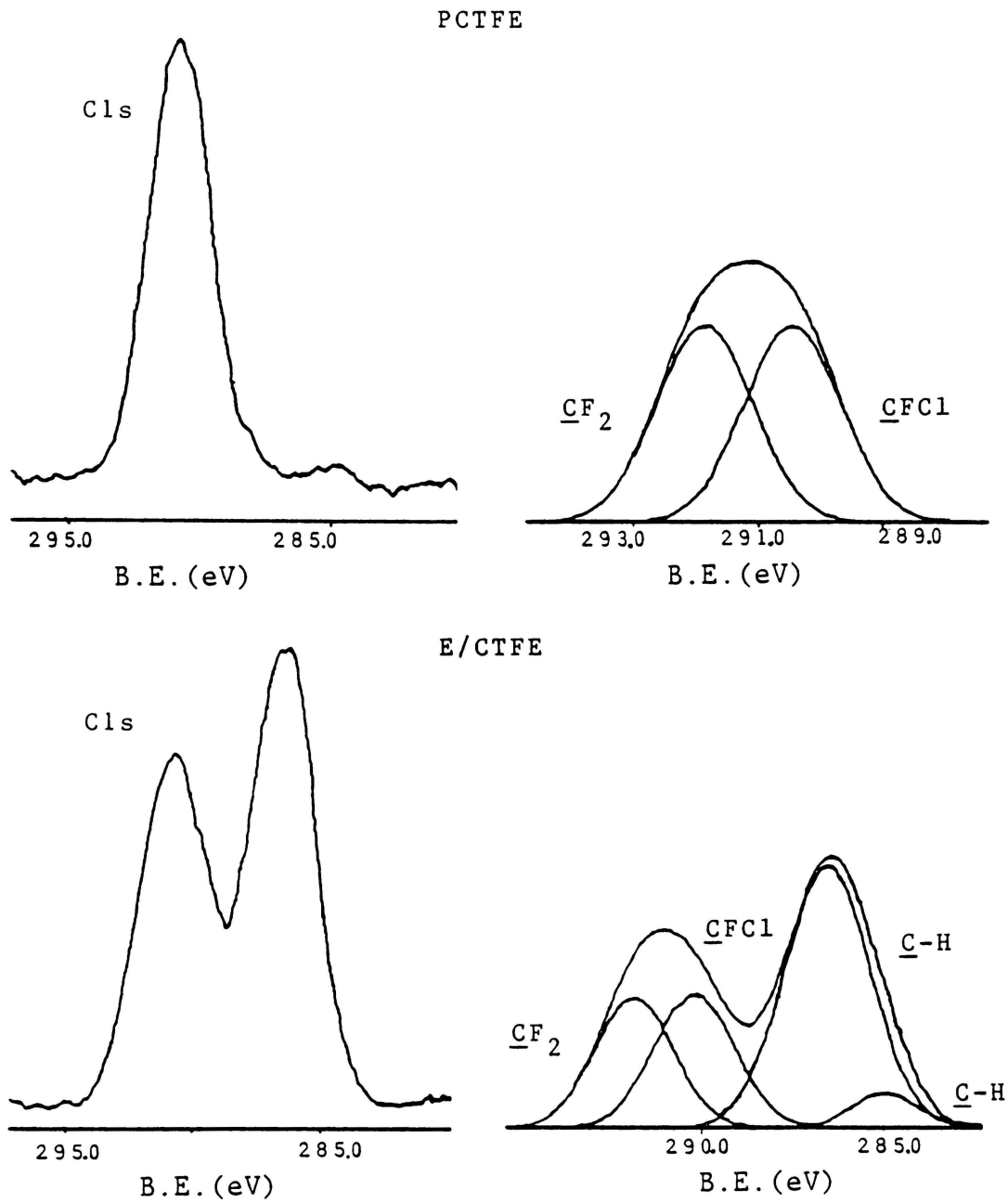

Figure 27: C1s, F1s and C12p spectra of PCTFE and E/CTFE polymers with corresponding curve-fitted spectra.

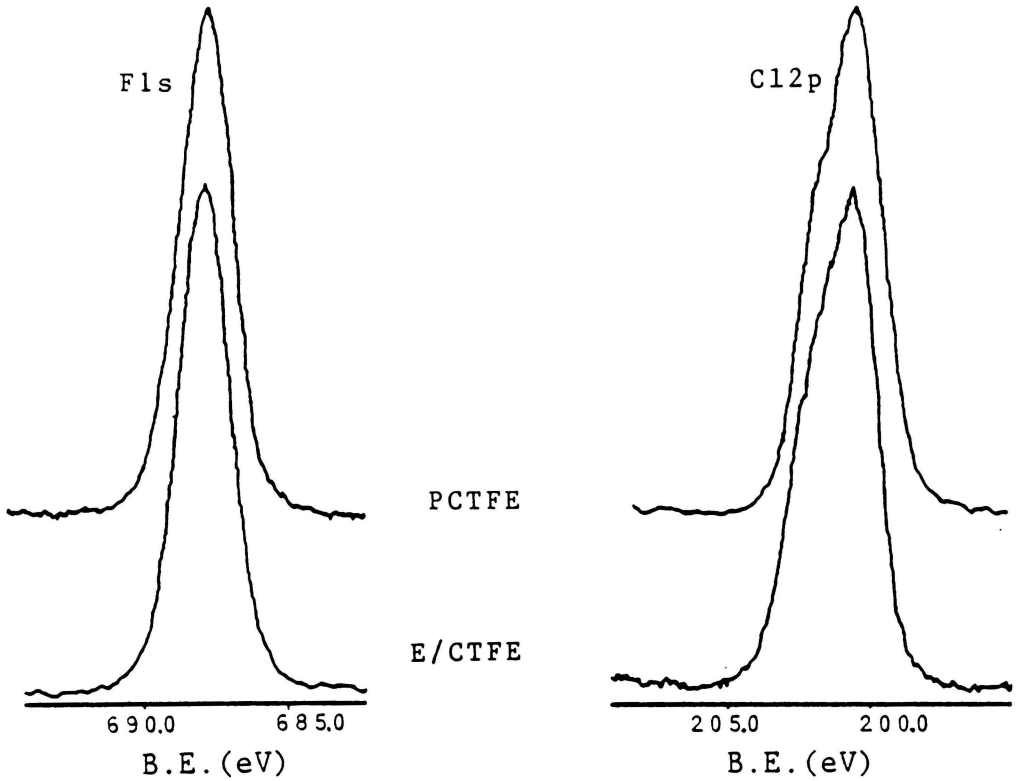

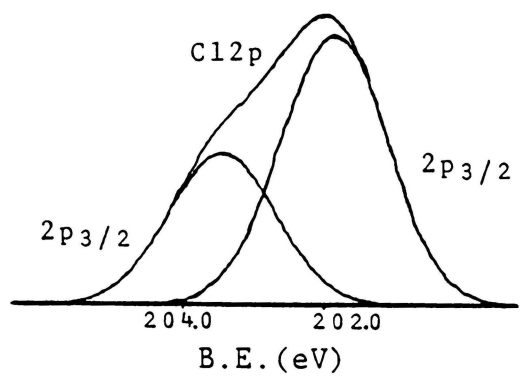

Figure 27: Continued.

TABLE 10

Core level binding energies (eV.) of PCTFE and E/CTFE.

Polymer	C1s*	F1s*	C12p*
PCTFE	290.4 291.8	689.2	200.5 202.1
E/CTFE	285.0 286.5 290.3 291.6	689.0	200.5 202.1

* $\Delta E = \pm 0.2$ eV.

- Bands located in the range 21-17 eV. correspond to the superposition of C-C bands with Cl3s orbital bands.
- At BE = 14.3 eV. are bands attributed to C-F linkages.
- Bands corresponding to F2p orbitals are observed at BE = 10.5 eV.
- Bands located at 6.6 eV. pertain the Clπ lone pair formed by contribution of the Cl3p orbitals.

Some differences between the valence bands of PCTFE and E/CTFE are observed. Specifically, bands corresponding to the superposition of C-C bands and Cl3s orbital bands are more intense for the copolymer and shifted towards higher binding energy, that is, towards bands concerning the C-C bonds involved in the ethylene units. In addition, the Cl3p band at 6.6 eV. is less intense in the copolymer. This is easily rationalized in terms of the higher relative concentration of C-C bonds present in the E/CTFE copolymer, as opposed to PCTFE. The observed differences illustrate the fingerprint characteristic of the valence energy level spectra.

The angle dependent XPS data is presented in Figure 29 in terms of a plot of F1s/C1s and Cl2p/C1s ratios as functions of the electron exit angle for both polymers. For PCTFE, both ratios remain constant when the exit angle is decreased, indicating a "clean" surface. The F1s/C1s and Cl2p/C1s ratios corresponding to E/CTFE decrease as the exit

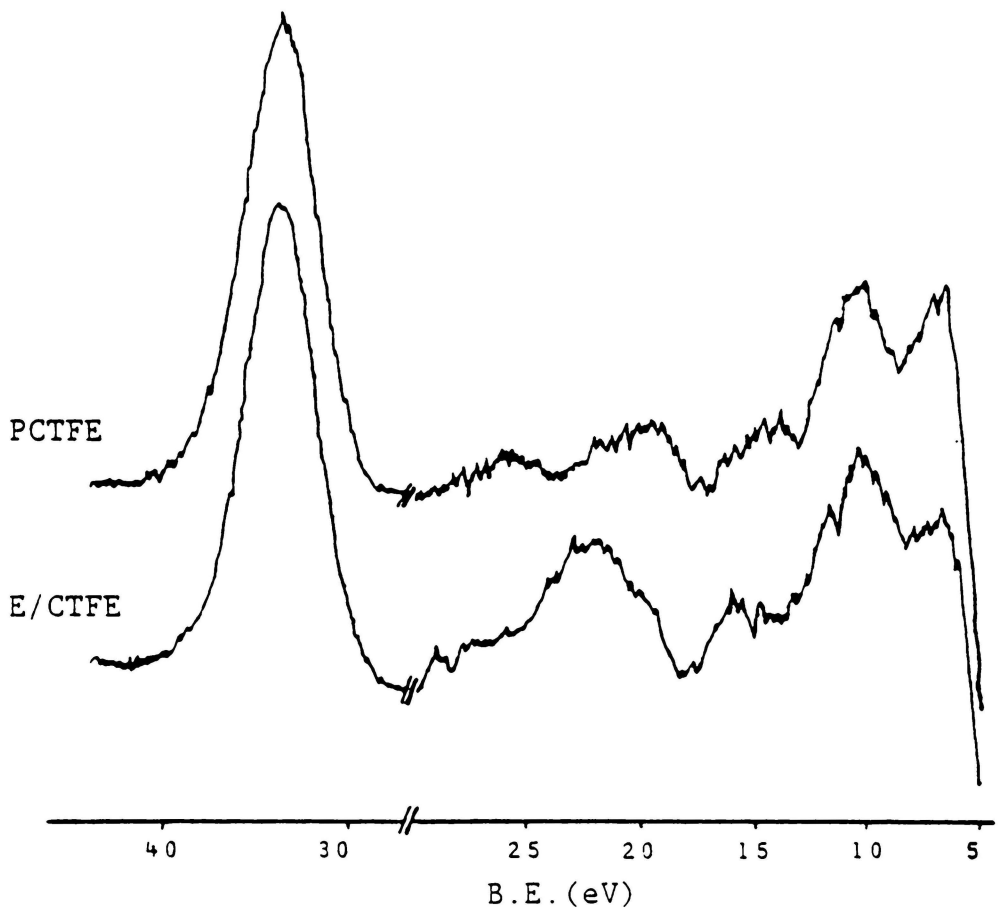

Figure 28: Valence energy level spectra of PCTFE and E/CTFE.

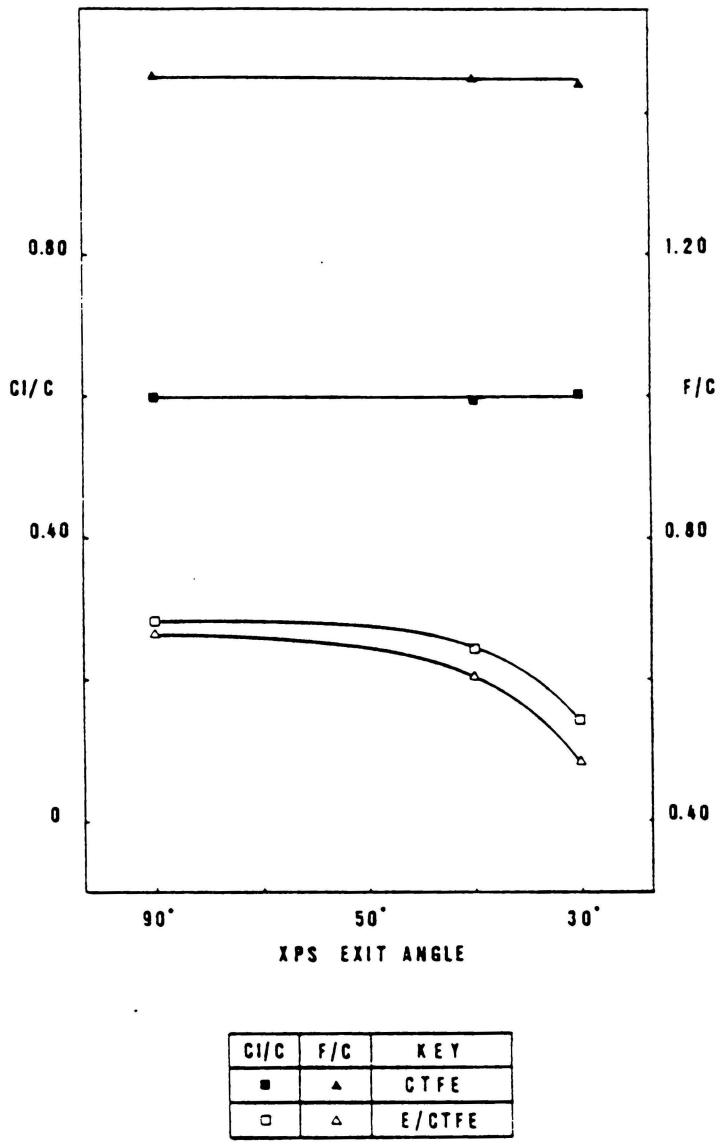

Figure 29: Graph of F1s/C1s and C12p/C1s intensity ratios of PCTFE and E/CTFE.

angle is decreased. Since the contribution of carbonaceous contamination to the C1s peak was substracted from the total C1s spectrum area, the data suggest a preferential orientation of the ethylene segments closer to the surface than the CTFE units. The largest change in the ratios occurs at the lower exit angles, i.e. when the outermost atom layers are probed. Therefore, the arrangement of the ethylene segments is very close to the surface of the polymer. Based on these observations and considering the crystalline nature of the polymer, a schematic representation of the atomic ordering at the surface of the polymer can be constructed as shown in Figure 30. These results are not surprising if the critical surface tensions of the two homopolymers PE and PCTFE are considered. Since PE has γ_{PE} = 28 dyn.cm^{-1} and γ_{PCTFE} = 31 dyn.cm^{-1} [36], the preferential orientation of the ethylene segments close to the surface can be expected.

Based on the angle dependent XPS results discussed, it may be anticipated that block copolymers of E/CTFE would present ethylene blocks phase segregated towards the surface of the polymer.

It is noteworthy to mention some comments about the effects that surface contamination can exert in surface analysis by discussing data obtained for two commercial samples. Prior to the analysis of laboratory samples, PCTFE

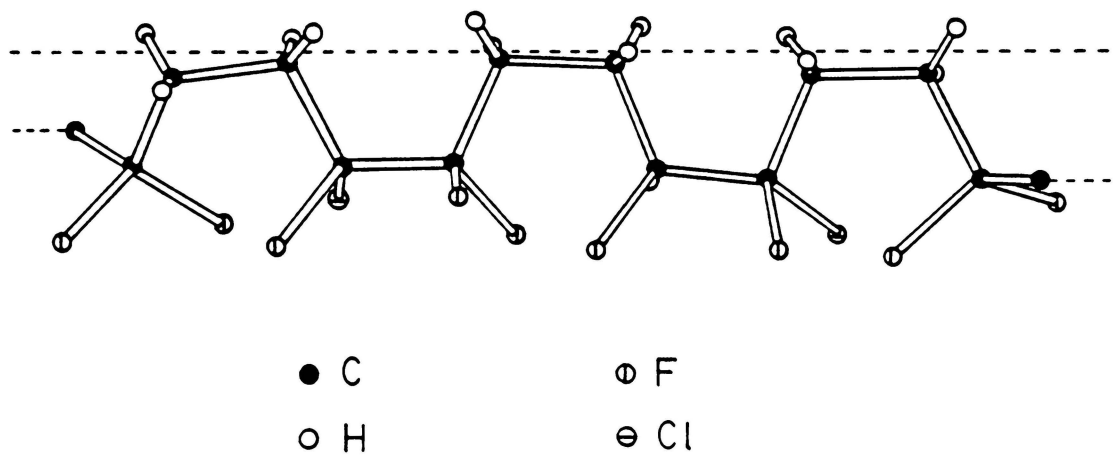

Figure 30: Model of E/CTFE atomic arrangement on the surface of a 1:1 alternating copolymer.

and E/CTFE 1:1 alternating polymers provided by an industrial source were subjected to XPS surface analysis. These commercial samples showed oxygen contamination. Figure 31 presents the angular-dependent XPS data obtained for the commercial polymers showing oxygen contamination. The data are presented in the same form as in Figure 28, i.e. F1s/C1s and Cl2p/C1s ratios as functions of the electron exit angle. Both, F1s/C1s and Cl2p/C1s ratios corresponding to PCTFE decrease as the exit angle is decreased. This is not consistent with the homogeneous surface composition that is obtained when a pure PCTFE sample is analyzed. Therefore, the chemical composition and atomic arrangement at the surface of the polymer is changed. In addition, the F1s/C1s and Cl2p/C1s ratios of the copolymer have the same value for a given electron exit angle, not consistent with the chemical composition of the copolymer units.

As shown by the example above, the information obtained from samples slightly contaminated can strongly affect the results obtained from surface analysis, and even more important is the change that can occur in the surface properties of the polymers. Consequently, if a particular application of the polymer is based on its surface characteristics, a very small concentration of contamination can cause the failure of the polymer in that particular application. However, fast and simple, XPS analysis can

provide information regarding this matter. Therefore, the value of XPS as a routine industrial analytical tool is shown by the example.

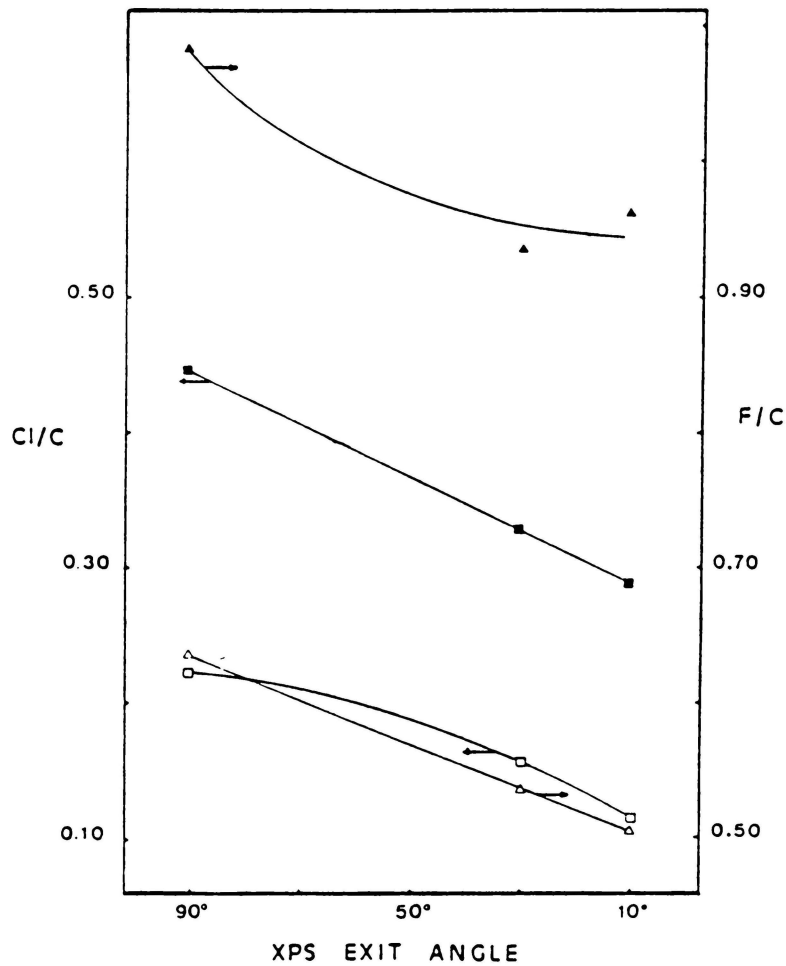

Figure 31: Graph of F1s/C1s and C12p/C1s ratios of commercial PCTFE and E/CTFE polymers.

POLYURETHANES

In this section, the data of polymers comprising the fourth group are analyzed. A comparative analysis of specimens from the "bulk" and surface of each polyurethane is performed. The term surface was already defined in the Introduction. Whereas, "bulk" is defined in this section as the fresh surface created by "slicing" a sample immediately prior to introduction into the analysis chamber.

In Figure 32 an XPS wide scan spectrum representative of a polyurethane is shown. The C1s, O1s and N1s photoelectron lines can be observed at binding energies of 285 eV., 532 eV. and 400 eV., respectively. Figure 33 presents the core energy level spectra corresponding to ether estane, ester estane and solithane based polyurethane. Figure 34 depicts the computer curve-fitted spectra corresponding to the C1s and O1s photoelectron lines of the three polyurethanes. Table 11 shows the binding energies measured for these polymers. As shown in Figures 33 and 34, and Table 11, the C1s spectra present three component peaks. At BE = 285.0 eV. the superposition of C-H and C-N bonds is observed, a component corresponding to carbon singly bonded to oxygen is located at BE = 286.5 eV. and at BE = 289.1 eV. is the carbon doubly bonded to oxygen component. Although the binding energies are in agreement within ±0.2 eV. for the three polyurethanes, different line profiles are

observed. The curve-fitted spectra shown in Figure 34 bring out the different intensities of the C1s component peaks for the polyurethanes. Ether estane presents the lowest intensity C=O component and the highest intensity C-O component, consistent with the high concentration of ether segments (soft segments). Ester estane has the highest relative intensity C=O component of this group, in agreement with the presence of the tetramethylene adipate soft segments. Solithane based polyurethane shows a C=O component of intermediate intensity. The O1s spectra also show these differences due to the chemical structure of the polyurethanes. For example, ether estane presents a very high intensity O-C component at BE = 531.9 eV. Whereas, the C=O component is barely observed at BE = 533.5 eV. Ester estane and solithane based polyurethane show O-C and O=C components of similar intensity as observed in the curve-fitted spectra in Figure 34. The N1s spectrum located at BE = 400.2 eV. is a symmetrical peak of low intensity in the three polyurethanes.

In Table 12 the angle-dependent XPS data for "bulk" and surface specimens are presented in terms of O1s/C1s and N1s/C1s relative intensity ratios. The depth profile of a surface specimen of ether estane shows that the O1s/C1s ratio remains approximately constant as the surface is approached. However, the N1s/C1s ratio decreases strongly as

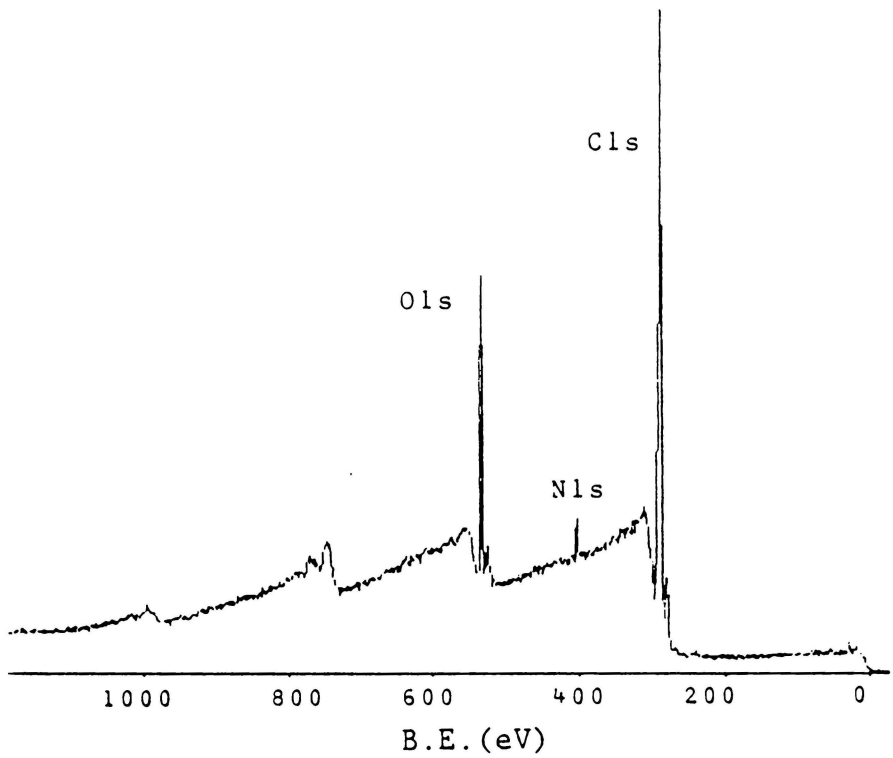

Figure 32: Representative XPS wide scan spectra for the polyurethanes.

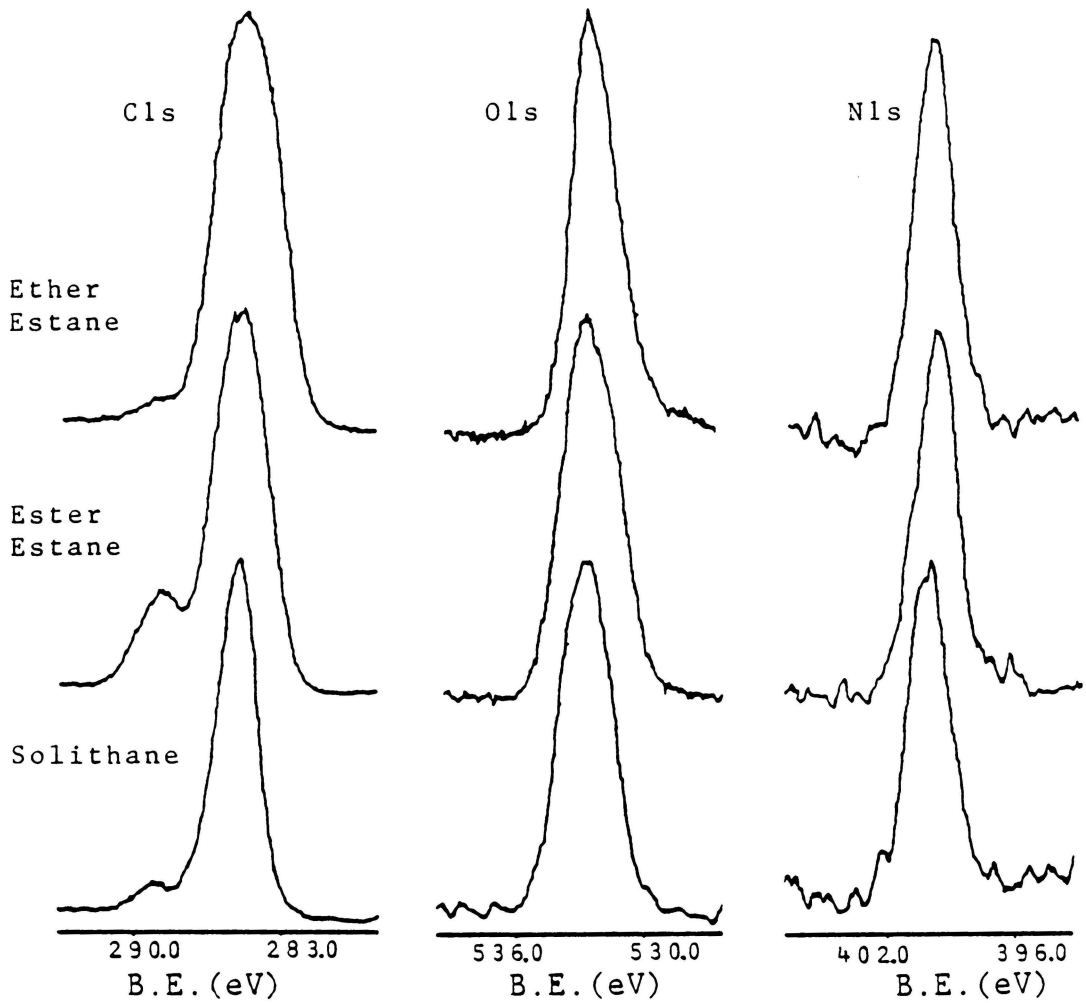

Figure 33: C1s, O1s and N1s spectra corresponding to the polyurethanes.

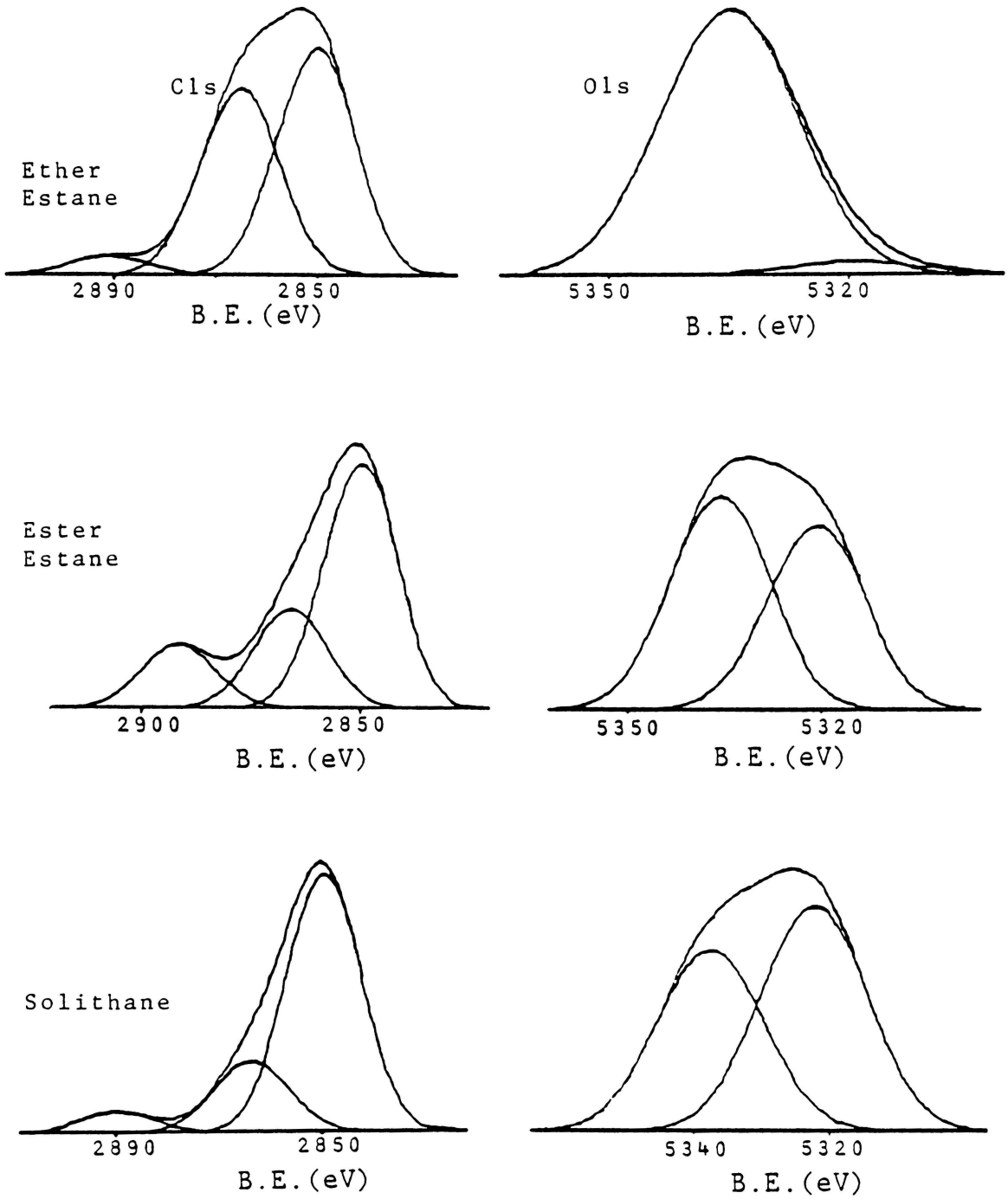

Figure 34: Curve-fitted spectra of polyurethanes.

TABLE 11

Core level binding energies (eV.) corresponding to the polyurethanes.

Polymer	C1s*	O1s*	N1s*
Ether Estane	285.0 286.6 289.1	531.9 533.5	400.3
Ester Estane	285.0 286.6 289.2	531.9 533.5	400.2
Solithane	285.0 286.5 289.0	532.1 533.7	400.0

* $\Delta E = \pm 0.2$ eV.

the electron exit angle is decreased. These data indicates that the concentration of oxygen relative to carbon does not change in the few outermost atom layers, whereas the concentration of nitrogen decreases. Since only the hard segments of the polyurethane (MDI) contain nitrogen, the data indicate that the hard segments are segregated towards the bulk of the specimen. The stoichiometric O/C ratio of the soft segments is 0.25, whereas, the N/C ratio of the hard segments is 0.13. Since the O/C ratio determined for this polyurethane is less than 0.25 and nitrogen is detected at grazing exit angle, the ether segments do not form an overlayer at the surface. Instead, both segments are present in the outermost atom layers with a higher concentration of ether segments, as opposed to block copolymers with poly (dimethyl siloxane) in which PDMS forms an overlayer at the surface[44]. The "bulk" specimen of ether estane also presents constant O1s/C1s ratio and decreasing N1s/C1s ratio as the exit angle is decreased, indicating the preferential segregation of the hard segments towards the bulk of the sample. These results, in addition to the results obtained for the surface, are consistent with a domain-like morphology that occurs not only in the bulk, but also at the surface. However, the domain dimensions are very small as opposed to PDMS domains observed in block copolymers by Patel[44]. Based on the mechanical properties and dichroism

data, Seymour et al.[108,109] proposed such a model for the bulk morphology of ether and ester estane in which a domain-like structure is present with characteristic domain dimensions of less than 50Å.

The angular-dependent data corresponding to the surface of ester estane show constant O1s/C1s and decreasing N1s/C1s ratios as the electron exit angle is decreased. Consequently, the surface of ester estane is enriched with ester soft segments. The same results are obtained when a "bulk" specimen is analyzed. The results can be rationalized in the same lines of ether estane.

The depth profile of the surface of the solithane based polyurethane presents O1s/C1s and N1s/C1s ratios that are constant when the electron exit angle is decreased. That is, the surface composition is constant throughout the XPS analytical depth. These results can be rationalized considering that the solithane based polyurethane is a crosslinked polyurethane. Apparently, the cross-links act as anchoring sites not allowing the segregation of the soft segments at the surface. This hypothesis is somewhat asserted by the results obtained for the "bulk" specimen of this polyurethane. The "bulk" specimen shows a constant O1s/C1s ratio. However, the N1s/C1s ratio decreases as the electron exit angle is decreased, indicating depletion of hard segments from the few outermost angstroms of the

TABLE 12

Angle-dependent XPS data corresponding to polyurethanes.

		Bulk		Surface	
Polymer	Angle	O/C[a]	N/C[b]	O/C[a]	N/C[b]
Ether Estane	90°	0.200	0.038	0.220	0.052
	30°	0.200	0.029	0.210	0.040
	10°	0.190	0.016	0.210	0.012
Ester Estane	90°	0.240	0.040	0.280	0.041
	30°	0.230	0.026	0.277	0.030
	10°	0.230	0.013	0.270	0.018
Solithane	90°	0.140	0.040	0.140	0.044
	30°	0.130	0.023	0.130	0.041
	10°	0.140	0.015	0.130	0.042

a. $\Delta O/C = \pm 10\%$
b. $\Delta N/C = \pm 10\%$

sample. Since the "bulk" specimens are prepared by slicing the sample as described in Methods, the procedure would break the anchoring sites (crosslinks) causing diffusion of the soft segments towards the surface and the heterogeneous chemical composition observed in the "bulk" specimen. These speculations are in agreement with investigations performed by Ophir and Wilkes[110] on crosslinked polyurethanes, in which they found that the extent of domain formation was decreased by crosslinking.

The discussion of the XPS depth profiles for each polyurethane brings out the effect that crosslinking can exert on the surface chemical composition. Ether and ester estane are linear segmented polyurethanes. Both of them presented heterogeneous chemical compositions in the "bulk" and surface specimens that indicated a preferential segregation of the soft segments towards the outermost layers of the specimen. However, the solithane based polyurethane, a crosslinked polyurethane, shows such a heterogeneous chemical composition only in the sliced "bulk" specimen. Therefore, this indicates that the crosslinks do not allow the microphase segregation that takes place in the linear polyurethane to occur in solithane. Consequently, crosslinking of polymers can, not only cause important changes in the bulk properties, but also in the surface properties of polymers that need to be investigated.

Chapter VI

CONCLUSIONS

The present study indicates that some kind of ordering effect occurs in all the groups investigated, and that within a group the effect is reproducible. Depending on several factors, the ordering effect can be present in different forms, such as preferential segregation of a crystalline block to the surface, segregation of a component of different crystalline structure to the surface or simply orientation of a segment of the polymer towards the surface.

Poly (ethylene terephthalate) shows that as the order increases, the amount of crystalline cyclic oligomer increases at the surface. That is, as the degree of crystallinity of the PET matrix increases, the cyclic oligomers are forced out of the matrix towards the surface of the specimen.

The group composed by the block copolyesters presents the ordering effect in the form of preferential segregation of one crystalline group to the surface. Copolyesters containing saturated and unsaturated blocks show the saturated blocks preferentially segregated at the surface. Whereas the all aromatic copolyester has the VIIAR block (highest degree of conjugation) segregated to the surface.

In the fluorine containing polymers, crystalline E/CTFE alternating copolymer shows a conformation with the preferential orientation of ethylene groups closer to the surface than the CTFE units.

The polyurethane group presents the segregation of soft segments to the surface of the specimens. Linear segmented polyurethanes, ether and ester estane, show angular dependent XPS data consistent with a domain-like morphology with a higher concentration of soft segments at the surface. Solithane, a crosslinked polyurethane, does not present preferential segregation of any segments at the surface. However, nitrogen depletion is observed when a cut sample is analyzed. It is believed that crosslinking inhibits the preferential orientation of soft segments towards the surface of the polymer.

LITERATURE CITED

1. D.F.Kagan, V.V.Prokopenko, V.M.Malinskii, and N.F.Bakeyev, *Polym. Sci. U.S.S.R. 32, 124 (1972).*

2. M.J.Owens and J.Thompson, *British Polym. J. 4, 297 (1972).*

3. D.M.Brewis, in "*Surface Analysis and Pretreatment of Plastics and Metals*", *D.M.Brewis,Ed., 1982, p1.*

4. J.Schultz, K.C.Sehgal and M.E.R.Shanahan, *Adhesion 1, K.W.Allen, Ed., 1977, p269.*

5. P.O.Sherman, S.Smith and B.Jahannessen, *Textiles Res. J. 39, 449 (1969).*

6. D.J.Lyman, L.C.Metcalf, D.Albo Jr., K.F.Richards, and J.Lamb, *Trans. Amer. Soc. Artif. Int. Organs 20B, 474 (1974).*

7. R.E.Baier, V.LR.E.Baier, V.L.Gott, and A.Feruse, *Trans. Amer. Soc. Artif. Int. Organs 16, 50 (1970).*

8. D.J.Lyman, K.Knutson, B.McNeil, and K.Shibatani, *Trans. Amer. Soc. Artif. Int. Organs 21, 49 (1975).*

9. D.W.Dwight and W.M.Riggs, *J. Colloid and Interface Sci. 47, 3, 650 (1974).*

10. R.T.McBride and L.E.Wolinski (to DuPont), *U.S. Patent 3,296,011 (1967).*

11. D.M.Brewis and D.Briggs, *Polymer 22, 7 (1981).*

12. D.Briggs, D.G.Rance, C.R.Kendall and A.R.Blythe, *Polymer 21, 895 (1980).*

13. D.K.Owens, *J. Appl. Polym. Sci. 19, 3315 (1975).*

14. D.Allara, "*Photons - Useful probes of thin film and interface structure*". *Seminar VPI&SU, April 1984.*

15. J.D.Andrade, G.K.Iwamoto, and B.McNeill, in "*Advances in Characterization of Metal and Polymer Surfaces*",*L.H.Lee, Ed., Academic Press, NY, 1976, p.133.*

16. S.W.Graham and D.M.Hercules, *J. Biomed. Mat. Res. 15, 349 (1981).*

17. C.S.Paik Sung, C.B.Hu, E.W.Merril and E.W.Salzman, *J. Biomed. Mat. Res. 12, 791 (1978).*

18. C.S.Paik Sung and C.B.Hu, *J. Biomed. Mat. Res. 13, 161 (1979).*

19. C.S.Paik Sung and C.B.Hu, *J. Biomed. Mat. Res. 13, 45 (1979).*

20. E.Nyilas and R.S.Ward Jr., *J. Biomed. Mat. Res. Symp. 8, 69 (1977).*

21. S.W.Graham and D.M.Hercules, *J. Biomed. Mat. Res. 15, 465 (1981).*

22. B.D.Ratner, in *"Photon, Electron and Ion Probes of Polymeric Structure and Properties", D.W.Dwight, T.J.Fabish, and H.R.Thomas, Eds., ACS Symp. Ser. No. 162, ACS, Washington D.C., 1981, p371.*

23. S.I.Stupp, J.W.Kauffman and S.H.Carr, *J. Biomed. Mat. Res. 11, 237 (1977).*

24. D.J.Lyman, *Pure & Appl. Chem. 50, 427 (1978).*

25. K.Knutson and D.J.Lyman, *Org. Coat. Plast. Chem. 42, 621 (1980).*

26. K.Knutson and D.J.Lyman, *Polym. Sci. Tech. 14, 173 (1981).*

27. B.D.Ratner, P.K.Weathersby, A.S.Hoffman, M.A.Kelly, and L.H.Scharpen, *J. Appl. Polym. Sci. 22, 643 (1978).*

28. M.H.Litt and T.Matsuda, in *"Copolymers, Polyblends, and Composites", N.A.J.Platzer, Ed., Adv. Chem. Ser. No.142, ACS Washington D.C., 1975, p320.*

29. M.H.Litt, F.Rahl and L.G.Roldan, *J. Polym. Sci. Part A-2 7, 463 (1969).*

30. K.Kugo, Y.Hata, T.Hayashi, and A.Nakajima, *Polym. J. 14, 401 (1982).*

31. H.R.Thomas and J.J.O'Malley, *Macromolecules 12, 323 (1979).*

32. J.J.O'Malley, H.R.Thomas and G.M.Lee, *Macromolecules 12, 996 (1979).*

33. D.T.Clark, J.Peeling and J.M.O'Malley, *J. Polym. Sci.: Polym. Chem. Ed. 14, 543 (1976).*

34. J.Brandrup and E.H.Immergut, Eds., *Polymer Handbook, Interscience, New York (1966).*

35. W.A.Zisman, *Adv. Chem. Ser. 43, ACS Washington D.C. (1964), p1.*

36. H.R.Thomas and J.J.O'Malley, in *"Photon, Electron and Ion Probes of Polymer Structure and Properties", D.W.Dwight, T.J.Fabish and H.R.Thomas, Eds., ACS Symp. Ser. No. 162, 1981, p319.*

37. J.E.McGrath, D.W.Dwight, J.S.Riffle, T.F.Davidson, D.C.Webster,and R.Viswanatha, *Polym. Prepr. 20(2), 528 (1979).*

38. D.W.Dwight, B.Beck, J.S.Riffle, and J.E.McGrath, *Polym. Prepr. 20(1), 702 (1979).*

39. J.S.Riffle, *PhD. Dissertation, VPI & SU (1980).*

40. A.K.Sha'aban, *M.S. Thesis, VPI & SU (1983).*

41. A.K.Sha'aban et al., *Polym. Prepr., Div. Polym. Chem., ACS 24(2), 130 (1983).*

42. N.Patel, *M.S. Thesis, VPI & SU (1984).*

43. J.A.Gardella Jr., J.S.Chen, J.H.Magill and D.M.Hercules, *J. Am. Chem. Soc. 105, 4536 (1983).*

44. K.H.Garner, J.H.Magill and E.D.T.Atkins, *Polymer 19, 370 (1978).*

45. A.Keller, E.Martucelli, J.Priest and Y.Udagawa, *J. Polym. Sci. Part A, 9, 1807 (1971).*

46. J.G.Dillard, D.W.Dwight,H.R.Thomas, J.P.Wightman, *"Electron Spectroscopy: Principles and Practice. An ACS short course.", 1980.*

47. C.D.Wagner, W.M.Riggs, L.E.Davis, J.F.Moulder, G.E.Muilenberg , *"Handbook of X-ray Photoelectron Spectroscopy." Perkin-Elmer Corp. (1979).*

48. D.T.Clark, in *"Handbook of X-ray and Ultraviolet Photoelectron Spectroscopy.",D.Briggs, ed., Heyden & Son Ltd., 1978, p.211.*

49. C.D.Wagner, in "*Handbook of X-ray and Ultraviolet Photoelectron Spectroscopy.*",*D.Briggs, Ed., Heyden & Son Ltd., 1978, p.249.*

50. R.H.Thomas, *PhD Thesis, "The application of ESCA to structure and Bonding in Selected Polymeric Systems.", University of Durham, U.K. (1977).*

51. D.Briggs, in "*Electron Spectroscopy: Theory, Techniques and Applications.", C.R. Brundle and A.D.Baker, Editors, Academic Press, NY, 1979, Vol.3., p.306.*

52. K.Siegbahn et al., *ESCA-Atomic Molecular and Solid State Structure Studied by Means of Electron Spectroscopy, Nova. Act. Regiae, Soc. Sci. Upsaliensis Ser.IV, Vol. 20 (1967).*

53. T.A.Carlson, *Photoelectron and Auger Spectroscopy, Plenum Press, NY, 1975.*

54. D.T.Clark, "*Handbook of X-ray and Ultraviolet Photoelectron Spectroscopy."D.T.Briggs, Ed., Heyden & Son Ltd., 1978, p.211.*

55. A.Dilks, "*Electron Spectroscopy: Theory, Techniques and Applications.", C.C.Brundle and A.D.Baker, Ed., Academic Press, NY, 1981, Vol.4, p.278.*

56. R.Manne, T.Aberg, *J. Chem. Phys. Lett. 7, 282 (1970).*

57. D.T.Clark, I.Scanlan and J.Muller, *Theor. Chim. Acta 35, 341 (1974).*

58. D.T.Clark, A.Dilks, *J. Polym. Sci., Polym. Chem. 14, 533 (1976).*

59. D.T.Clark, A.Dilks, *J. Polym. Sci., Polym. Chem. 15, 15 (1977).*

60. D.T.Clark, D.B.Adams, J.Peeling, H.R.Thomas, *J. Electron. Spectrosc. 8, 51 (1976).*

61. a) J.M.Andre, J.Delhalle, S.Delhalle, R.Caudano, J.J.Pireaux and J.J.Verbist, *Chem. Phys. Lett. 23, 206 (1973)*, b) J.Delhalle, J.M.Andre, S.Delhalle, J.J.Pireaux, R.Caudano and J.J.Verbist, *J. Chem. Phys. 60, 595 (1974)*, c) J.Delhalle, J.M.Andre, S.Delhalle, J.J.Pireaux, R.Caudano and J.J.Verbist, *J. Electron Spectrosc. 5, 531 (1974)*, d) J.Delhalle, S.Delhalle, J.M.Andre, J.J.Pireaux, J.Riga, R.Caudano andJ.J.Verbist, *J. Electron. Spectrosc. 12, 293 (1977).*

62. J.J.Pireaux, J.Riga, J.Caudano, J.J.Verbist, Y.Gobillon, J.Delhalle, S.Delhalle and J.M.Andre, *J. Polym. Sci., Polym.Chem. Ed. 17, 1175 (1979).*

63. a) D.T.Clark and H.R.Thomas, *J. Polym. Sci., Polym. Chem. Ed., 14,1671 (1976),* b) D.T.Clark and H.R.Thomas, *J. Polym. Sci., Polym. Chem. Ed., 14,1701 (1976).*

64. J.J.Pireaux, J.Riga, R.Caudano, J.Verbist, J.Delhalle, S.Delhalle, J.M.Andre, Y.Gabillon, *Phys. Scripta 16, 329 (1977).*

65. J.Delhalle, R.Montigny, C.Demanet and J.M.Andre, *Theoret. Chim. Acta (Berl.) 50, 343 (1979).*

66. J.M.Andre, J.Delhalle and J.J.Pireaux, "*Photon, Electron and Ion Probes of Polymeric Structure and Properties.*" *D.W.Dwight, T.J.Fabish and H.R.Thomas, Eds., ACS Symp. Ser. 162, ACS, Washington D.C. (1981), p.151.*

67. J.J.Pireaux, J.Riga, R.Caudano and J.Verbist, "*Photon, Electron, and Ion Probes of Polymeric Structures andProperties.*", *D.W.Dwight, T.J.Fabish and H.R.Thomas, Eds.,ACS Symp. Ser. 162, ACS, Washington D.C. (1981), p.169.*

68. E.S.Brandt, et al., *J. Elec. Spec. Rel. Phen. 14,113 (1978).*

69. P.Swift, *Surf. Interf. Anal. 4, 47 (1982).*

70. C.D.Wagner, *Anal. Chem. 44, 1050 (1972).*

71. C.D.Wagner, L.E.Davis, M.V.Zeller, J.A.Taylor, R.H. Raymond and L.H.Gale, *Surf. Interf. Anal. 3, 211 (1981).*

72. a) C.K.Jorgensen and H.Berthou, *Far. Disc. 54, 269 (1973),* b) H.Berthou and C.K.Jorgensen, *Anal. Chem. 47, 482 (1975),* c) H.Berthou and C.K.Jorgensen, *J. Elect. Spec. Rel. Phen. 5, 953 (1974).*

73. C.S.Fadley, "*Progress in Solid State Chemistry.*", *G.Somorjai and J.McCaldin, Eds.Pergamon Press, NY, 1976, Vol II, p.265.*

74. P.W.Palmberg, *Anal. Chem. 45, 549A (1973).*

75. H.Ebel and M.F.Ebel, "*X-ray Spectrometry.*", *Vol. 2, p.19 (1973).*

76. C.S.Fadley, R.J.Baird, W.Siekhaus, T.Novakov and S.A.L.Bergstrom, *J. Elect. Spec. Rel. Phen. 4, 93 (1974).*

77. H.E.Bishop and J.C.Riviere, *J. Appl. Phys. 40, 1740 (1969).*

78. C.S.Fadley, "*Electron Spectroscopy:Theory, Techniques and Applications.*", *C.S.Brundle and A.D.Baker, Eds., Academic Press, London, 1978, Vol. 2, p.1.*

79. J.H.Scofield, *J. Elect. Spec. Rel. Phen. 8, 129 (1976).*

80. a) V.I.Nefedov, N.P.Sergushin, J.M.Band and M.B.Trzhaskovskaya, *J. Elect. Spec. Rel. Phen. 2, 383 (1973).* b) V.I.Nefedov, N.P.Sergushin, Y.V.Salyn, I.M.Band and M.B.Trzhaskovskaya, *J. Elect. Spect. Rel. Phen. 7, 175 (1975).*

81. R.S.Reilman, A.Msezane and S.T.Manson, *J. Elect. Spec. Rel. Phen. 8, 389 (1976).*

82. C.J.Powell, *Surf. Sci. 44, 29 (1974).*

83. D.R..Penn, *J. Elect. Spec. Rel. Phen. 9, 29 (1976).*

84. M.P.Seah and W.A.Dench, *Surf. Interf. Anal. 1, 2 (1979).*

85. C.D.Wagner, L.E.Davis and W.M.Riggs, *Surf. Interf. Anal. 2, 53 (1980).*

86. J.Szajman and R.C.G.Leckey, *J.Elect. Spec. Rel. Phen. 23, 83 (1981).*

87. J.Szajman, J.Liesegang, J.G.Jenkin and R.C.G.Leckey, *J. Elect. Spec. Rel. Phen. 23, 97 (1981).*

88. J.C.Ashley and C.J.Tung, *Surf. Interf. Anal. 4, 52 (1982).*

89. C.E.Kuyatt, "*Methods of Experimental Physics.*", *L.Marton, Ed.,Academic Press, NY,1968Vol. 7A, p.16.*

90. A.Barrie, "*Handbook of X-ray and Ultraviolet Photoelectron Spectroscopy.*",*D.Briggs, Ed., Heyden, London, 1977, p.79.*

91. A.E.Hughes and C.C.Phillips, *Surf. Interf. Anal. 4, 220 (1982).*

92. a) C.S.Fadley and S.A.L.Bergstrom, *Phys. Letters 35A, 375 (1971),* b) C.S.Fadley and S.A.L.Bergstrom, *"Electron Spectroscopy.", D.A.Shirley, Ed., North Holland, Amsterdam,1972, p. 233.*

93. W.A.Fraser, J.V.Florio, W.N.Delgass and W.D.Robertson, *Surf. Sci. 36, 661 (1973).*

94. D.T.Clark, A.Dills, D.shuttleworth and H.R.Thomas, *J. Electr. Spec. Rel. Phen. 14, 247 (1978).*

95. M.B.Polk et al., *Macromolecules 14, 1626 (1981).*

96. M.B.Polk et al., *Macromolecules 17,129 (1984).*

97. M.B.Polk et al., *J. Macrom. Sci., in press*

98. D.W.Dwight, J.E.McGrath and J.P.Wightman, *J. App. Polym. Sci.:App. Polym. Symp. 34, 35 (1978).*

99. A.Perovic and P.R.Sundaravajan, *Polymer Bulletin 6, 277 (1982).*

100. B.E.Mills and D.A.Shirley, *J. Am. Chem. Soc. 99, 5885 (1977).*

101. D.T.Clark, *"Advance Polymer Friction and Wear.", L.H.Lee, Ed., Plenum Press,1975, Vol. 5A, p.241.*

102. R.W.Seymour, G.M.Estes and S.L.Cooper, *Macromolecules 3, 579 (1970).*

103. G.M.Estes, R.W.Seymour and S.L.Cooper, *Macromolecules 4, 452 (1971).*

104. Z.H.Ophir and G.L.Wilkes, *Polym. Prep. Am. Chem. Soc. Div. Polym. Chem. 19(1), 26 (1978).*

The vita has been removed from the scanned document